

## Electronic Supporting Information

### Multivalent Polyrotaxane Vectors as Adaptive Cargo Complexes for Gene Therapy

Rodinel Ardeleanu<sup>a</sup>, Andrei I. Dascalu<sup>a</sup>, Andrei Neamtu<sup>a,b</sup>, Dragos Peptanariu<sup>a</sup>, Cristina M. Uritu<sup>a</sup>, Stelian S. Maier<sup>a,c</sup>, Alina Nicolescu<sup>a</sup>, Bogdan C. Simionescu<sup>a,d</sup>, Mihail Barboiu<sup>e</sup>, Mariana Pinteala<sup>a\*</sup>

#### Table of contents

<b>1. Chemical syntheses</b> .....	S4
<b>1.1. Synthesis and characterization of acrylated <math>\beta</math>-cyclodextrin <math>\beta</math>-CD</b> .....	S4
<i>Figure S1.</i> Schematic representation of $\beta$ -CD esterification with acryloyl chloride.....	S4
<i>Figure S2.</i> <sup>1</sup> H-NMR spectra of native $\beta$ -CD (bottom) and of acrylated $\beta$ -CD (top).....	S5
<i>Figure S3.</i> <sup>1</sup> H, <sup>13</sup> C-HSQC spectrum of the acrylated $\beta$ -CD, recorded in DMSO-d <sub>6</sub> .....	S6
<i>Figure S4.</i> <sup>13</sup> C-NMR spectra of native $\beta$ -CD (bottom) and of acrylated $\beta$ -CD (top, recorded on a 10 mm probe), recorded in DMSO-d <sub>6</sub> .....	S7
<i>Figure S5.</i> FT-IR spectra of the unmodified $\beta$ -CD and of the acrylated $\beta$ -CD.....	S8
<b>1.2. Preparation of <math>\alpha,\omega</math>-bis(propargyloxy)poly(ethylene glycol)</b> .....	S8
<i>Figure S6.</i> Schematic representation of PEG etherification with propargyl bromide.....	S8
<i>Figure S7.</i> <sup>1</sup> H-NMR spectrum of $\alpha,\omega$ -bis-(propargyloxy)-PEG <sub>1000</sub> recorded in DMSO-d <sub>6</sub> .....	S9
<i>Figure S8.</i> <sup>13</sup> C-NMR spectrum of $\alpha,\omega$ -bis-(propargyloxy)-PEG <sub>1000</sub> recorded in DMSO-d <sub>6</sub> .....	S10
<i>Figure S9.</i> FT-IR spectra of $\alpha,\omega$ -bis-(propargyloxy)-PEG <sub>1000</sub> .....	S10
<b>1.3. Synthesis of 1-(3-bromopropyl)silatrane and 1(3-azidopropyl)silatrane</b> .....	S11
<b>1.3.1. Synthesis of 1-(3-bromopropyl)silatrane</b> .....	S11
<i>Figure S10.</i> Schematic representation of 1-(3-bromopropyl)silatrane synthesis.....	S11
<i>Figure S11.</i> <sup>1</sup> H-NMR spectrum of 1-(3-bromopropyl)silatrane, recorded in DMSO-d <sub>6</sub> ..	S12
<i>Figure S12.</i> <sup>13</sup> C-NMR spectrum of 1-(3-bromopropyl)silatrane, recorded in DMSO-d <sub>6</sub> .....	S12

<b>Figure S13.</b> FT-IR spectra of 1-(3-bromopropyl)silatrane.....	S13
<b>1.3.2. Synthesis of 1-(3-azidopropyl)silatrane.....</b>	S13
<b>Figure S14.</b> Schematic representation of 1-(3-azidopropyl)silatrane synthesis.....	S13
<b>Figure S15.</b> <sup>1</sup> H-NMR spectrum of 1-(3-azidopropyl)silatrane recorded in DMSO-d <sub>6</sub> ...	S14
<b>Figure S16.</b> <sup>13</sup> C-NMR spectrum of 1-(3-azidopropyl)silatrane recorded in DMSO-d <sub>6</sub> ...	S15
<b>Figure S17.</b> FT-IR spectra of 1-(3-azidopropyl)silatrane.....	S15
<b>1.4. Synthesis of <math>\alpha,\omega</math>-bis(propargyloxy)poly(ethylene glycol)/acrylated <math>\beta</math>-CD poly(pseudorotaxane).....</b>	S16
<b>Figure S18.</b> Schematic representation of $\alpha,\omega$ -bis-(propargyloxy)-PEG <sub>1000</sub> /acrylated $\beta$ -CD poly(pseudorotaxane) preparation.....	S16
<b>Figure S19.</b> <sup>1</sup> H-NMR spectrum of the prepared $\alpha,\omega$ -bis-(propargyloxy)-PEG <sub>1000</sub> /acrylated $\beta$ -CD poly(pseudorotaxane), recorded in DMSO-d <sub>6</sub> .....	S17
<b>Figure S20.</b> FT-IR spectra of $\alpha,\omega$ -bis-(propargyloxy)-PEG <sub>1000</sub> /acrylated $\beta$ -CD poly(pseudorotaxane).....	S18
<b>1.5. Preparation of <math>\alpha,\omega</math>-bis-{1-[3-(silatranyl)prop-1-yl]-1H-1,2,3-triazol-5-yl}-PEG<sub>1000</sub>/acrylated <math>\beta</math>-CD polyrotaxane (ROT).....</b>	S18
<b>Figure S21.</b> Schematic representation of $\alpha,\omega$ -bis-{1-[3-(silatranyl)prop-1-yl]-1H-1,2,3-triazol-5-yl}-PEG <sub>1000</sub> /acrylated $\beta$ -CD polyrotaxane synthesis procedure.....	S18
<b>Figure S22.</b> <sup>1</sup> H-NMR spectrum of the capped ROT, recorded in DMSO-d <sub>6</sub> .....	S19
<b>Figure S23.</b> FT-IR spectra of $\alpha,\omega$ -bis-{1-[3-(silatranyl)prop-1-yl]-1H-1,2,3-triazol-5-yl}-PEG <sub>1000</sub> /acrylated $\beta$ -CD polyrotaxane.....	S19
<b>1.6. Preparation of PEI decorated polyrotaxane (ROT-PEI).....</b>	S20
<b>Figure S24.</b> Schematic representation of ROT-PEI preparation.....	S20
<b>Figure S25.</b> <sup>1</sup> H-NMR spectrum of ROT-PEI, recorded in D <sub>2</sub> O.....	S20
<b>Figure S26.</b> The GPC curve of ROT-PEI product in water.....	S21
<b>1.7. Preparation of PEI and PEG<sub>750</sub> decorated polyrotaxane (ROT-PEI-PEG<sub>750</sub>)....</b>	S21
<b>Figure S27.</b> Schematic representation of ROT-PEI-PEG <sub>750</sub> preparation.....	S21
<b>Figure S28.</b> <sup>1</sup> H-NMR spectra of A) ROT-PEI and B) ROT-PEI-PEG <sub>750</sub> , both recorded in D <sub>2</sub> O.....	S22

<b>Figure S29.</b> FT-IR spectrum of ROT-PEI-PEG <sub>750</sub> .....	S23
<b>1.8. Preparation of arginine decorated ROT-PEI (ROT-PEI-Arg)</b> .....	S23
<b>Figure S30.</b> General reaction pathway of ROT-PEI-Arg and ROT-PEI-G preparation...	S23
<b>Figure S31.</b> <sup>1</sup> H-NMR spectrum of ROT-PEI-Arg, recorded in D <sub>2</sub> O.....	S24
<b>1.9. Preparation of guanidine decorated ROT-PEI (ROT-PEI-G)</b> .....	S24
<b>Figure S32.</b> <sup>1</sup> H, <sup>13</sup> C-HMBC spectrum of ROT-PEI-G, recorded in D <sub>2</sub> O.....	S24
<b>2. Elemental analysis of the investigated carriers</b> .....	S25
<b>Table S1.</b> Elemental composition of the investigated carriers [mass %].....	S25
<b>3. In silico chemical modeling</b> .....	S26
<b>Figure S33.</b> (A) Moment of inertia (MOI) variation during the production molecular dynamics simulation, as a measure of system equilibration. (B) Snapshot of the structure of the polyrotaxane aggregate at the end of the 10 ns MD simulation.....	S26
<b>4. The efficacy of carriers – dsDNA electrostatic complexation (Gel retardation assay)</b> .....	S27
<b>Figure S34.</b> Gel retardation assay of ROT-PEI/pDNA, ROT PEI PEG750/pDNA, ROT PEI-G/pDNA, ROT PEI Arg/pDNA polyplexes at various N/P ratios from 1 to 60.....	S27
<b>5. Cytotoxicity assay</b> .....	S28
<b>Figure S35.</b> The results of cytotoxicity tests in the series of investigated transfection agents.....	S28
<b>6. Transfection efficacy tests</b> .....	S29
<b>Figure S36.</b> Fluorescence microcopy images of GFP-transfected cells, using ROT-PEI/pGFP, ROT-PEI-PEG <sub>750</sub> /pGFP, ROT-PEI-G/pGFP, ROT-PEI-Arg/pGFP and PEI (2 kDa)/pGFP as transfection agents, at all tested N/P ratios (from 5 to 80).....	S29
<b>7. Zeta potential measurements of polyplexes</b> .....	S30
<b>Figure S37.</b> The zeta potential variation of ROT-PEI/pDNA, ROT-PEI-PEG <sub>750</sub> /pDNA, ROT-PEI-G/pDNA and ROT-PEI-Arg/pDNA polyplexes.....	S30
<b>8. Transmission electron microscopy (TEM)</b> .....	S31
<b>Figure S38.</b> TEM images of ROT-PEI/pDNA, ROT-PEI-PEG <sub>750</sub> /pDNA, ROT-PEI-G/pDNA and ROT-PEI-Arg/pDNA polyplexes.....	S31
<b>Figure S39.</b> Size distribution of polyplex particles, obtained at N/P ratios of maximum transfection efficiency, according to TEM data.....	S32
<b>9. Size measurements by Dynamic Light Scattering (DLS) analysis</b> .....	S33

<b>Table S2.</b> Sizes of ROT-PEI/pDNA, ROT-PEI-PEG <sub>750</sub> /pDNA, ROT-PEI-G/pDNA and ROT-PEI-Arg/pDNA polyplexes obtained by DLS.....	S33
<b>10. The <i>in silico</i> estimation of the volume of cargocomplexes</b> .....	S34
<b>Figure S40.</b> The results of the calculation Van der Waals lateral surfaces enclosing the ROT-PEI polyrotaxane carrier, and the Dickerson-Drew DNA dodecamer.....	S34

## 1. Chemical syntheses

### 1.1. Synthesis and characterization of acrylated $\beta$ -cyclodextrin $\beta$ -CD

The first step in the development of the vector consisted in the insertion of acryloyl groups (Figure S1) onto the minor rim of  $\beta$ -cyclodextrin cavity (primary hydroxyl groups OH-6).

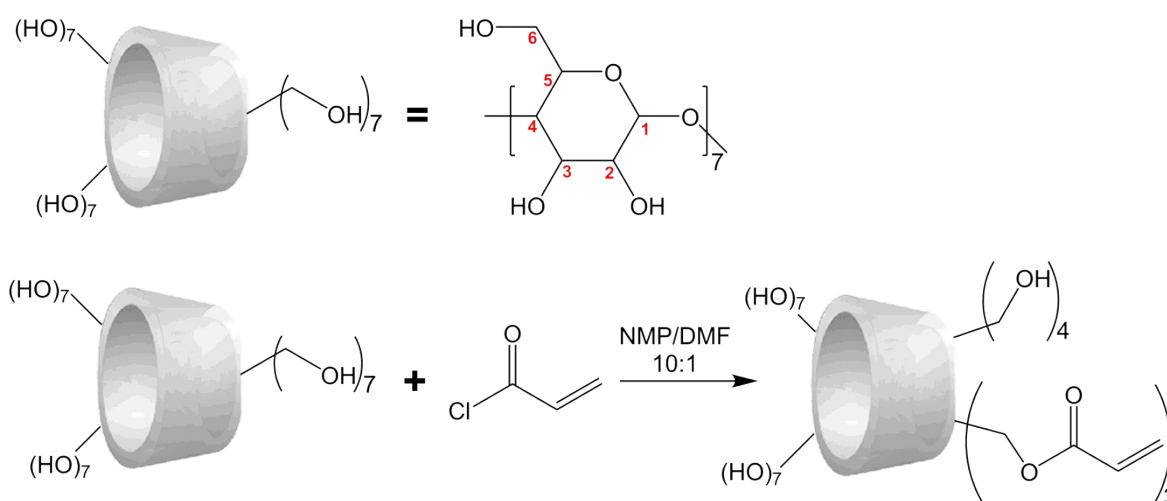


**Figure S1.** Schematic representation of  $\beta$ -CD esterification with acryloyl chloride.

Initially, the dried  $\beta$ -CD (10.00 g, 8.8 mmol) ( $M_w$  1134.98 Da) was dissolved in anhydrous N-methyl-2-pyrrolidone NMP (50 mL).<sup>1</sup> Following the complete dissolution of the  $\beta$ -CD, the flask was cooled in an ice bath, then the acryloyl chloride (2.86 mL, 3.18 g, 35.2 mmol) ( $M_w$  90.51 Da, density 1.114 g/mL at 25 °C) was dissolved in anhydrous DMF (5.0 mL) and added drop wise in the flask, under nitrogen atmosphere.<sup>[23]</sup> The molar ratio between the two reactants was 1:4  $\beta$ -CD : acryloyl chloride, and an excess coefficient of 1.33 was found necessary to ensure a maximal substitution degree, near to three. The reaction flask was maintained in the ice bath and stirred for 2 h. The reaction was continued for five days at

room temperature. Further, the reaction mixture was added drop wise in a buffer solution (250 mL, pH 7.0) to precipitate the acrylated product. Following the complete precipitation, the solid product was filtered, washed twice with deionized water and dried under vacuum. The crude solid product was twice recrystallized from methanol and dried under vacuum. The final product (9.48 g; yield 83.0 %) is soluble in methanol, acetone and tetrahydrofuran. According to elemental analysis, 42.85% of the primary hydroxyl groups (OH-6) of  $\beta$ -CD were esterified in the final product, which is equivalent to a substitution degree of 3.0 ( $M_w$  1297 Da).

$^1\text{H-NMR}$  (DMSO- $d_6$ , 400.13 MHz,  $\delta_{\text{H}}$  (ppm)): 3.40 (bs, H-2, H-4), 3.64 (bs, H-3), 3.86 (bs, H-5, H-6 from unmodified units), 4.16-4.64 (m, H-6 from modified units, OH-6), 4.88-5.00 (m, H-1), 5.84-6.25 (m,  $\text{CH}_2=\text{CH}-$ , OH-2, OH-3).

$^{13}\text{C-NMR}$  (DMSO- $d_6$ , 100.61 MHz,  $\delta_{\text{C}}$  (ppm)): 44.7-45.2 (C-6 in unmodified glucose units), 63.5-64.3 (C-6 in esterified glucose units), 69.2-72.9 (C-2, C-3, C-5), 80.9-83.4 (C-4), 101.5-102.4 (C-1), 127.8 ( $-\text{CH}=\text{}$ ), 131.6-132.0 ( $\text{CH}_2=\text{}$ ), 165.2-165.5 ( $-\text{C}=\text{O}$ ).

The severe broadening of all  $^1\text{H-NMR}$  signals, caused by the lack of symmetry of the modified  $\beta$ -CD, makes signal assignments a complicated task. In the  $^1\text{H-NMR}$  spectrum (Figure S2), the acrylic moiety has a distinctive set of signals assigned at 5.84 – 5.92 and 6.24 - 6.36 ppm, the protons of the  $\text{CH}_2=\text{}$  groups, and 6.11-6.25 ppm, the protons of the  $-\text{CH}=\text{}$  groups.

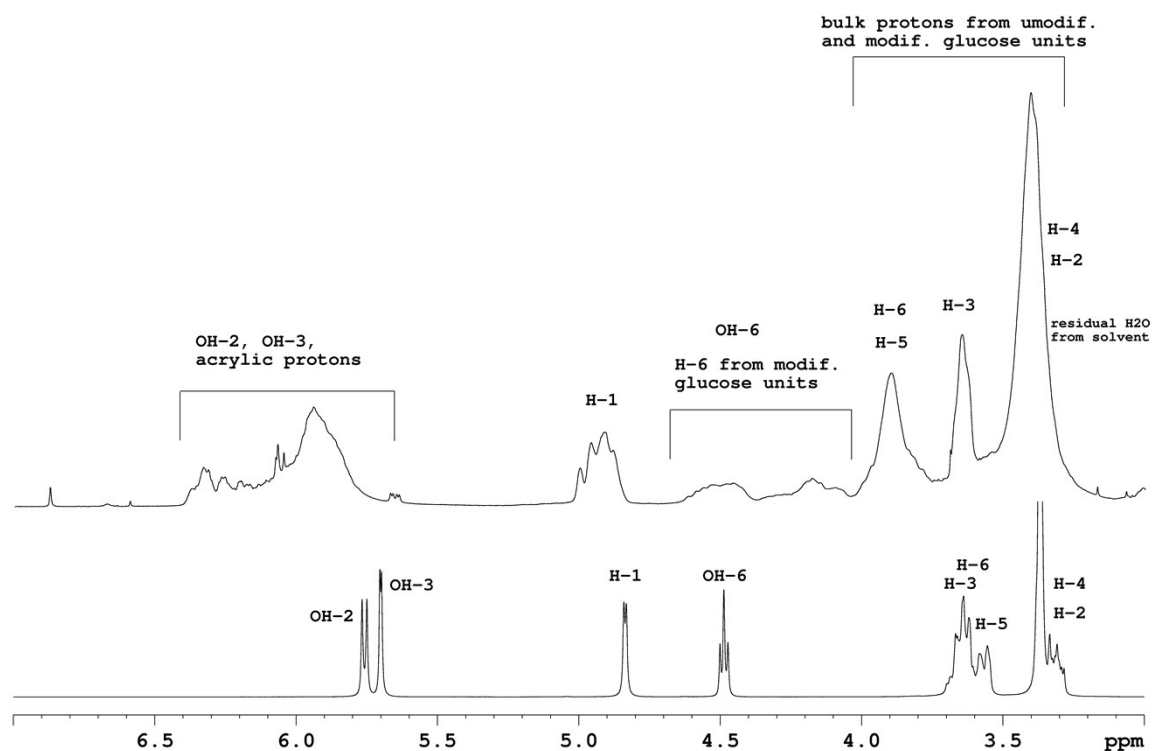


**Figure S2.** <sup>1</sup>H-NMR spectra of native β-CD (bottom) and of acrylated β-CD (top). Both spectra are recorded in DMSO-d<sub>6</sub>.

Since in the same spectral region there are signals corresponding to OH-2 and OH-3 from cyclodextrin, the exact assignments of the acrylic protons were done based on the correlations obtained from the <sup>1</sup>H,<sup>13</sup>C HSQC-NMR spectrum (Figure S3). In this type of experiment cross peaks appear due to the direct proton-carbon couplings. From the same <sup>1</sup>H,<sup>13</sup>C HSQC-NMR spectrum the set of signals from  $\delta = 4.16 - 4.28$  and  $\delta = 4.38 - 4.64$  ppm were assigned to the CH<sub>2</sub>-6 group from the modified glucose units. The signals for CH-2 and CH-3 do not suffer significant modifications, confirming the introduction of the acrylic groups only in position 6.

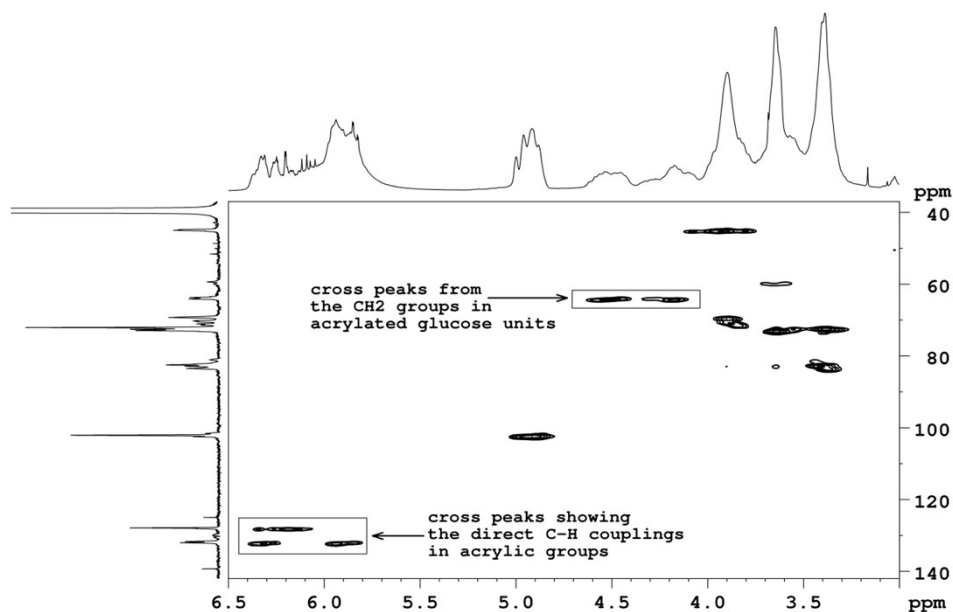


**Figure S3.**  $^1\text{H}, ^{13}\text{C}$ -HSQC spectrum of the acrylated  $\beta$ -CD, recorded in  $\text{DMSO-}d_6$ .

The  $^{13}\text{C}$ -NMR spectrum of the acrylated  $\beta$ -CD is also different from that of the native  $\beta$ -CD, all the signals characteristic to glucose units being split in groups of signals, suggesting that the seven glucose units are different (see Figure S4). The presence of acrylic group in position 6, induces a 20 ppm upfield shift of the signals corresponding to  $\text{CH}_2$ -6 groups from the unmodified glucose units. The acrylic groups have their characteristic signals at 127.8-128.1 ppm ( $-\text{CH}=\text{}$ ), 131.4-131.7 ppm ( $\text{CH}_2=\text{}$ ) and 165.1-165.5 ppm ( $\text{C}=\text{O}$ ). The rest of the signals are not influenced in a significant manner, appearing at the chemical shifts specific to  $\beta$ -CD.

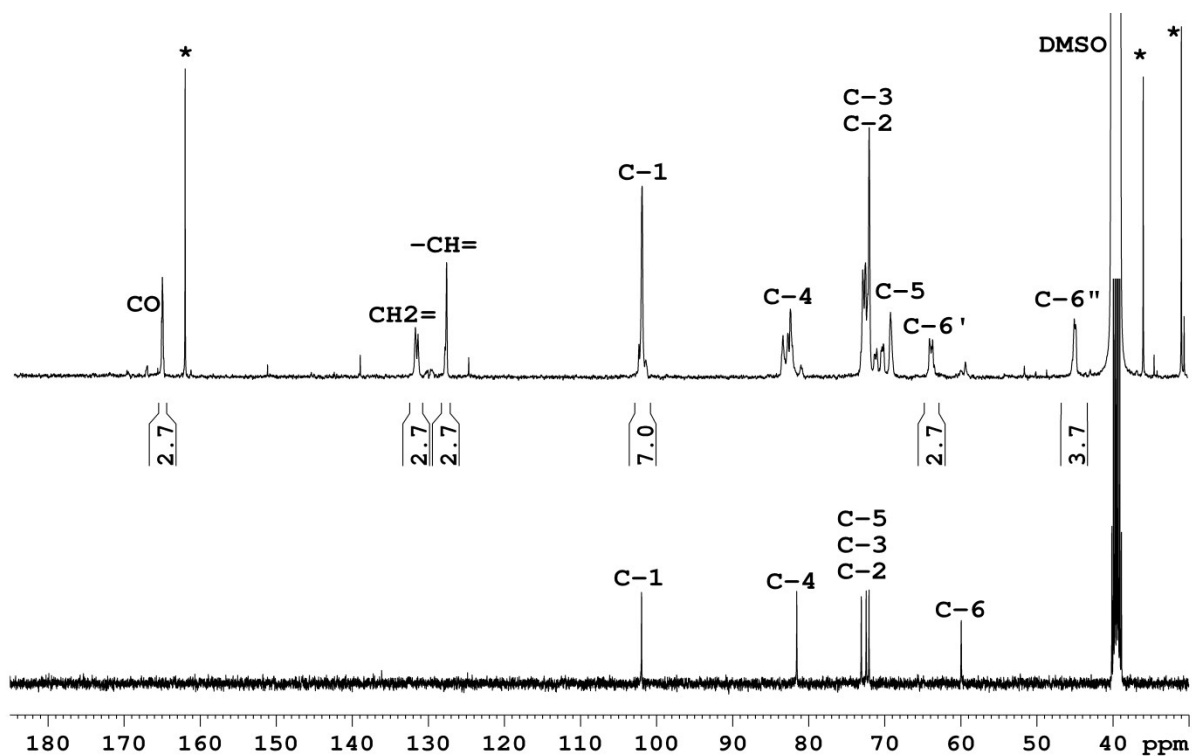


**Figure S4.**  $^{13}\text{C}$ -NMR spectra of native  $\beta$ -CD (bottom) and of acrylated  $\beta$ -CD (top, recorded on a 10 mm probe), recorded in DMSO- $d_6$ . The signals annotated with \* are from residual DMF, those with C-6' are the  $\text{CH}_2\text{-O}$  groups from modified glucose units and with C-6'' are the  $\text{CH}_2\text{-O}$  groups from unmodified glucose units.

The degree of substitution of the OH-6 groups of  $\beta$ -CD was estimated from semi-quantitative  $^{13}\text{C}$ -NMR data, acquired using 10,000 scans and 25 seconds for the relaxation delay (leading to 72 hours acquisition time on a 10 mm probe). Using these experimental conditions, we were able to determine a “semi-quantitative value” of 2.7 acrylic groups per 1  $\beta$ -CD molecule. This value resulted from the integrals ratio of the signals C-1 to CO, 7 : 2.7, as shown in Figure S4.

Figure S5 displays the FT-IR spectra of the unmodified  $\beta$ -CD and of the acrylated  $\beta$ -CD. A decrease in the intensity of OH vibration at  $3370\text{ cm}^{-1}$  was observed in the spectrum of acrylated  $\beta$ -CD, due to the decrease of hydroxyl groups as a consequence of the esterification reaction. The absorption band at  $1728\text{ cm}^{-1}$  is assigned to the vibration of  $\nu\text{ C=O}$  bonds in ester groups possessing  $\alpha$ - $\beta$  unsaturated carbon. The bands at  $1620\text{ cm}^{-1}$  ( $\nu\text{ C=C}$ ),  $1412\text{ cm}^{-1}$  ( $\nu\text{-HC=CH}_2\text{-}$ ) can be attributed to the vinyl groups in acrylated  $\beta$ -CD. Characteristic bands at  $1154\text{ cm}^{-1}$  due to  $\nu\text{-C-O-C-}$  in glycosidic bridges, and at  $1023\text{ cm}^{-1}$  (coupled  $\nu\text{ C-C}$  and  $\nu\text{ C-O}$ ) and  $1080\text{ cm}^{-1}$  due to  $\nu\text{ C-O}$  vicinal to the primary hydroxyl groups, were also observed.

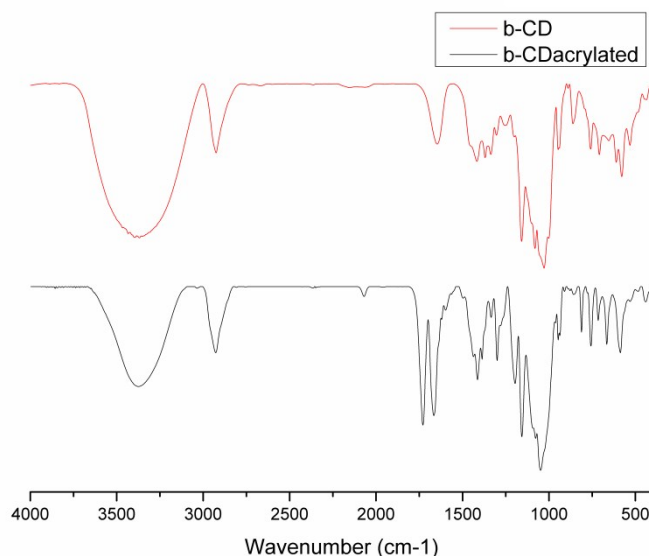


**Figure S5.** FT-IR spectra of the unmodified  $\beta$ -CD and of the acrylated  $\beta$ -CD.

## 1.2. Preparation of $\alpha,\omega$ -bis(propargyloxy)poly(ethylene glycol)

Poly(ethylene glycol) 1000 Da was initially dried at 100 °C and 20 mbar for 48 h. The complete removal of water was evaluated using thermogravimetric analysis. In a typical experiment (Figure S6), anhydrous PEG (10 g, 10 mmol) and sodium hydride NaH (0.72 g, 30 mmol) were dissolved in anhydrous THF (40 mL) in a 100 mL 3 neck flask equipped with a magnetic stirrer, ascending condenser, nitrogen inlet and dropping funnel. After two hours of stirring, the complete dissolution of the reagents was observed. In the next step, propargyl bromide (3.57 g, 30 mmol) was dissolved in anhydrous THF (7 mL) and added dropwise using the dropping funnel while the reaction flask was kept in an ice bath. After 2 h, the reaction flask was removed from the ice bath and the reaction was continued at room temperature. After 24 h the reaction mixture was subjected to distillation in order to remove the solvent and excess volatile reagents. The recrystallization from *n*-hexane afforded 9.5 g of  $\alpha,\omega$ -bis-(propargyloxy)-PEG<sub>1000</sub> (90% yield).

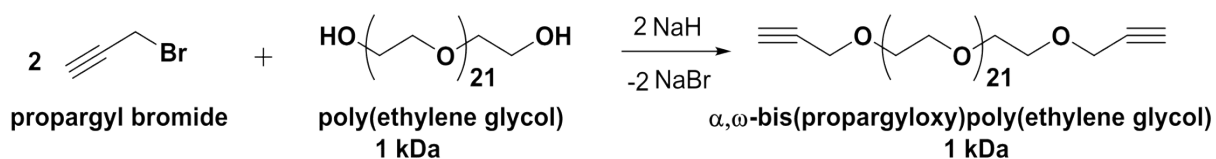


**Figure S6.** Schematic representation of PEG etherification with propargyl bromide.

$^1\text{H}$  NMR (DMSO- $d_6$ , 400.13 MHz,  $\delta$  (ppm)): 3.41 (2H, t, 2.3 Hz, CH-propargyl), 3.50-3.56 (all -O-CH<sub>2</sub>-CH<sub>2</sub>-O- from PEG), 4.15 (4H, d, 2.3 Hz, CH<sub>2</sub>-propargyl).

$^{13}\text{C}$  NMR (DMSO- $d_6$ , 100.61 MHz,  $\delta$  (ppm)): 57.4 (CH<sub>2</sub>-propargyl), 68.5, 69.5 and 69.7 (all -O-CH<sub>2</sub>-CH<sub>2</sub>-O- from PEG), 77.0 (CH-propargyl), 80.3 (C-propargyl).

The obtained PEG derivative was characterized through NMR spectroscopy. In the  $^1\text{H}$ -NMR spectrum (see Figure S7), the propargyl group has two signals: a triplet at 3.41 ppm and a doublet at 4.15 ppm. The multiplicity of the signals is due to the four bonds couplings between the CH and CH<sub>2</sub> protons. All the protons from the PEG moiety have a broad signal, centered at 3.52 ppm.

In the  $^{13}\text{C}$ -NMR spectrum (see Figure S8), the propargyl group is characterized by the presence of three signals: 57.4 ppm (CH<sub>2</sub>), 77.0 (CH) and 80.3 (C). The PEG moiety also has three distinctive signals: two less intense signals at 68.5 and 69.5 ppm, corresponding to CH<sub>2</sub> groups situated towards the end of the polymeric chain, and a more intense signal at 69.7 ppm, corresponding to the rest of the CH<sub>2</sub> groups.

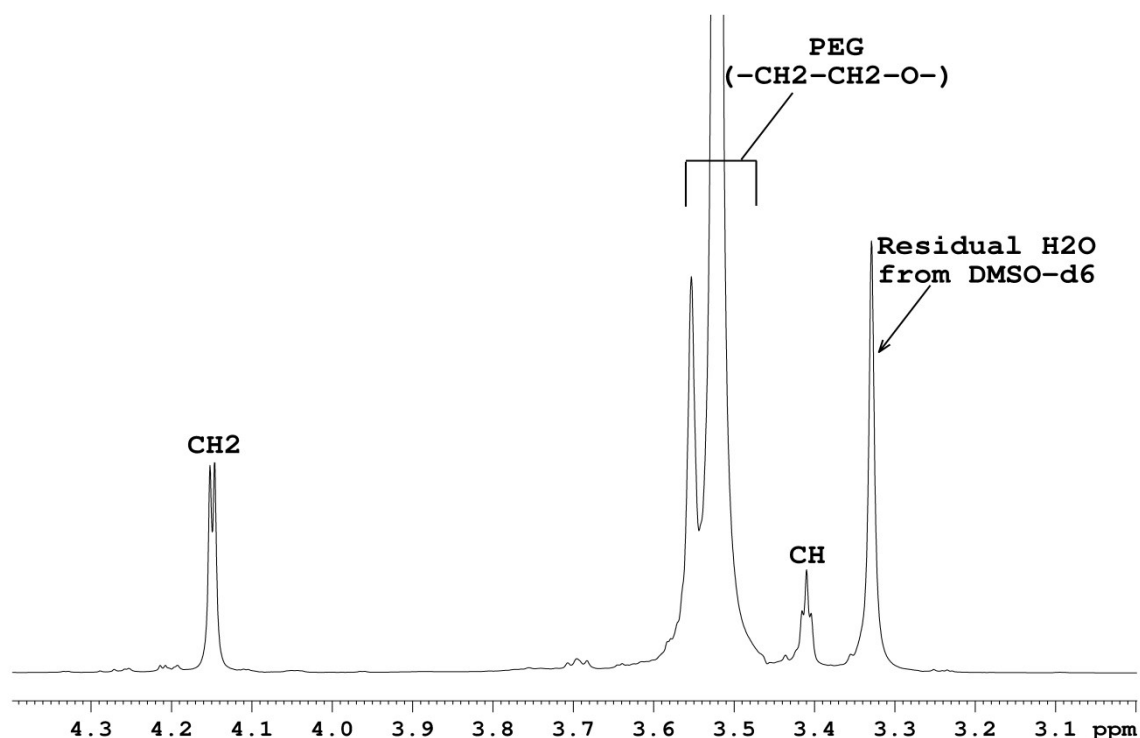


**Figure S7.**  $^1\text{H}$ -NMR spectrum of  $\alpha,\omega$ -bis-(propargyloxy)-PEG<sub>1000</sub> recorded in DMSO- $d_6$ .

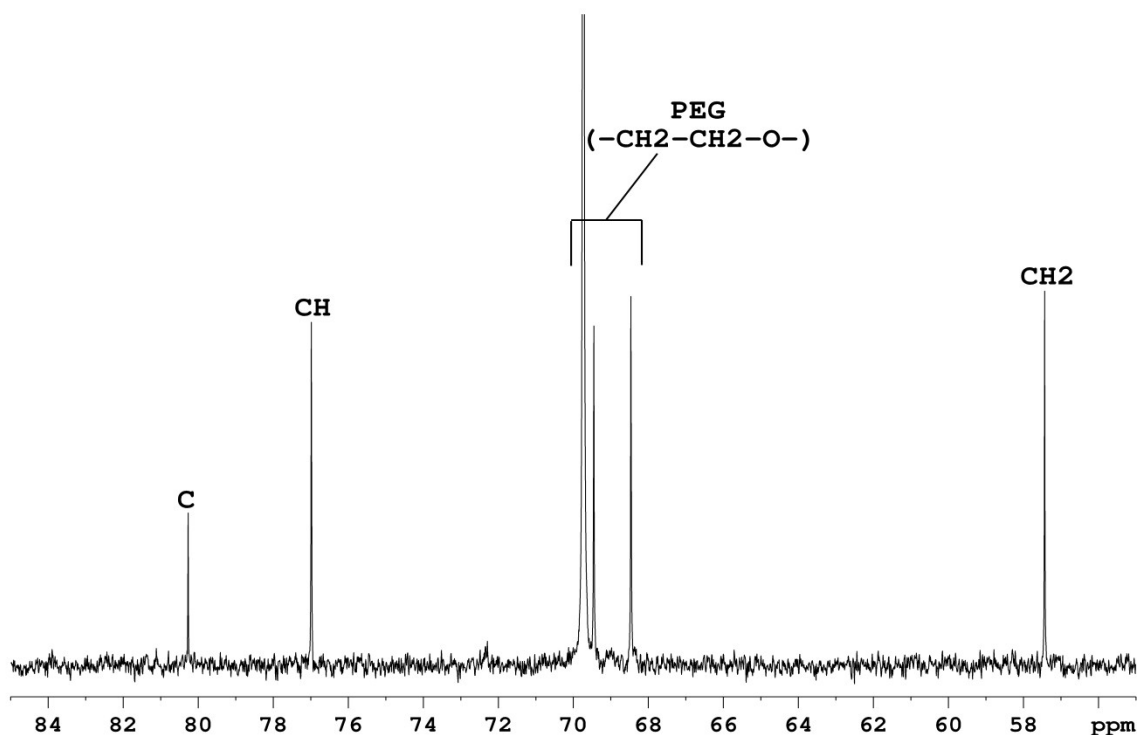


**Figure S8.**  $^{13}\text{C}$ -NMR spectrum of  $\alpha,\omega$ -bis-(propargyloxy)-PEG<sub>1000</sub> recorded in DMSO-*d*<sub>6</sub>.

The absence of the OH valence vibration at 3500-3700  $\text{cm}^{-1}$  in the FT-IR spectrum (Figure S9) of  $\alpha,\omega$ -bis(propargyloxy)poly(ethylene glycol) indicated the complete conversion of the starting hydroxyl groups to the desired propargyl ether analogues. This observation was supported by the presence of the band at 1099  $\text{cm}^{-1}$  specific to asymmetric vibration of C-O-C etheric group.

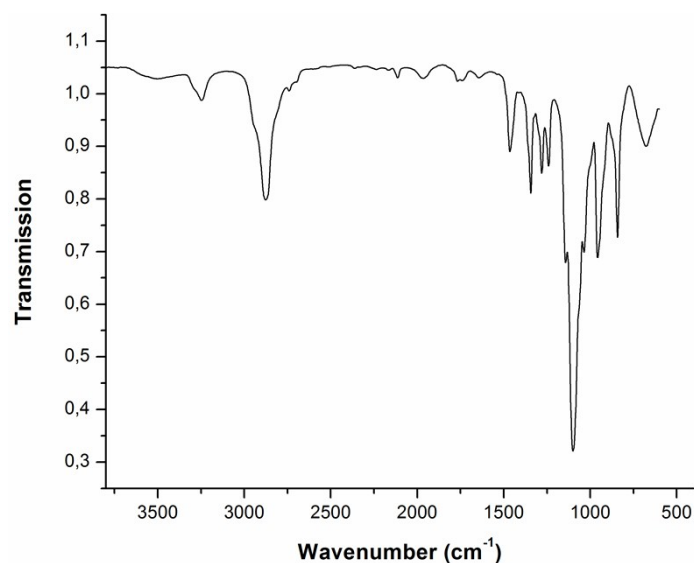


**Figure S9.** FT-IR spectra of  $\alpha,\omega$ -bis-(propargyloxy)-PEG<sub>1000</sub>.

### 1.3. Synthesis of 1-(3-bromopropyl)silatrane and 1-(3-azidopropyl)silatrane

#### 1.3.1. Synthesis of 1-(3-bromopropyl)silatrane

1-(3-bromopropyl)silatrane and 1-(3-azidopropyl)silatrane were prepared according with the procedures described in the literature.<sup>2</sup> In a typical experiment (Figure S10), triethanoleamine (10 g, 67 mmol) and potassium hydroxide (0.2 g, 3.5 mmol) were dissolved in toluene (40 ml) and mixed with 1-(3-bromopropyl)-trimethoxysilane (16.3 g, 67 mmol) at 80 °C. The desired product 1-(3-bromopropyl)silatrane was separated by vacuum distillation and subsequent recrystallization from chloroform, affording 10.52 g of transparent crystals (53% yield).

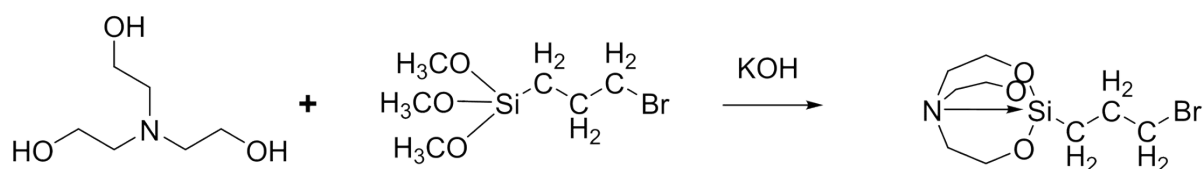


**Figure S10.** Schematic representation of 1-(3-bromopropyl)silatrane synthesis.

<sup>1</sup>H NMR (DMSO-d<sub>6</sub>, 400.13 MHz,  $\delta_{\text{H}}$  (ppm)): 0.22-0.26 (2H, m, CH<sub>2</sub>-Si), 1.76-1.84 (2H, m, CH<sub>2</sub>-CH<sub>2</sub>-Si), 2.79 (6H, t, 5.9 Hz, CH<sub>2</sub>-N), 3.41 (2H, t, 7.4 Hz, CH<sub>2</sub>-Br), 3.61 (6H, t, 5.9 Hz, CH<sub>2</sub>-O).

<sup>13</sup>C NMR (DMSO-d<sub>6</sub>, 100.61 MHz,  $\delta_{\text{C}}$  (ppm)): 16.4 (CH<sub>2</sub>-Si), 29.7 (CH<sub>2</sub>-CH<sub>2</sub>-Si), 39.2 (CH<sub>2</sub>-Br), 49.9 (CH<sub>2</sub>-N), 56.6 (CH<sub>2</sub>-O).

The obtained product was characterized by NMR spectroscopy. The absence from both <sup>1</sup>H and <sup>13</sup>C-NMR spectra of the signal corresponding to trimethoxy group indicates the formation of the new product. In the <sup>1</sup>H-NMR spectrum (see Figure S11), two triplets are observed, centered at 2.79 and 3.61 ppm, due to CH<sub>2</sub>-N and CH<sub>2</sub>-O, respectively. The propyl moiety has three characteristic signals as follows: two complex signals in the 0.22-0.26 and 1.76-1.84 ppm regions and one triplet centered at 3.41 ppm.

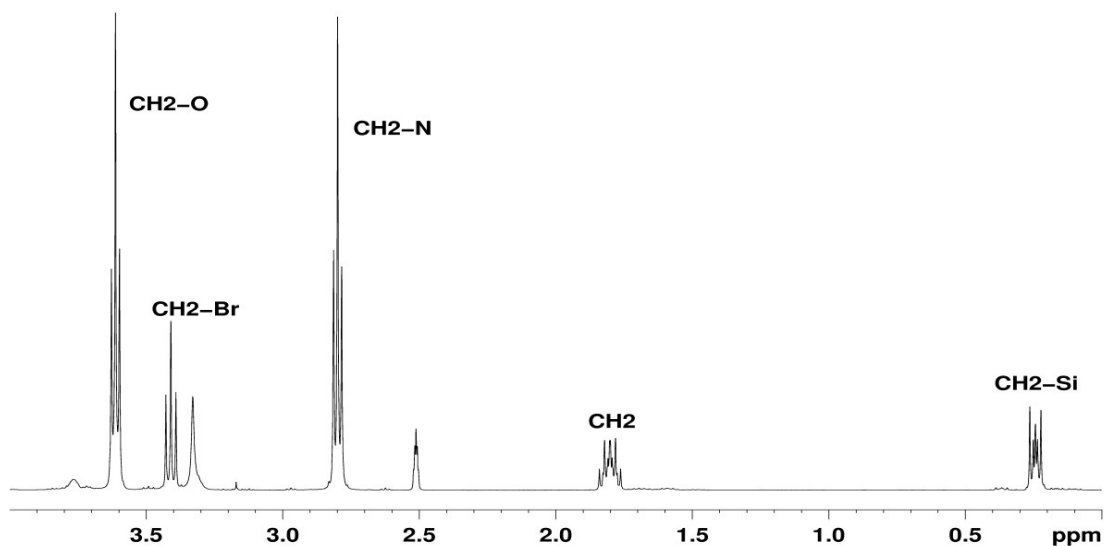


**Figure S11.**  $^1\text{H}$ -NMR spectrum of 1-(3-bromopropyl)silatrane, recorded in DMSO- $d_6$ .

In the  $^{13}\text{C}$ -NMR spectrum (see Figure S12), five signals are observed, one of them being partially overlapped by the solvent's signal. The most deshielded signals, at 56.6, 49.9 and 39.2 ppm, are due to  $\text{CH}_2\text{-O}$ ,  $\text{CH}_2\text{-N}$  and  $\text{CH}_2\text{-Br}$ , respectively. Due to the shielding effect exerted by the electrons of the silicon atom, the signal for  $\text{CH}_2$  directly linked to Si appears at 16.4 ppm.

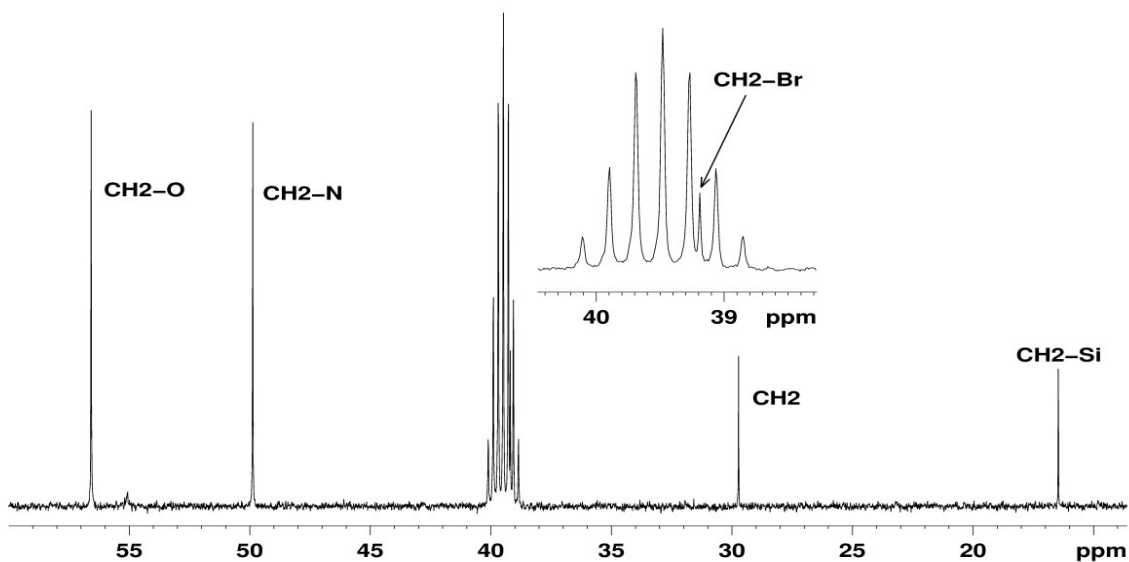


**Figure S12.**  $^{13}\text{C}$ -NMR spectrum of 1-(3-bromopropyl)silatrane, recorded in DMSO- $d_6$ .

The FT-IR spectra of the brominated cyclic derivative (Figure S13) indicated the presence of the characteristic bands at 1126, 1101  $\text{cm}^{-1}$  assigned to Si-O-C groups, alongside the characteristic vibrations at 565  $\text{cm}^{-1}$  (C-Br), 622  $\text{cm}^{-1}$  (Si-C), 874 and 910  $\text{cm}^{-1}$  (C-N).

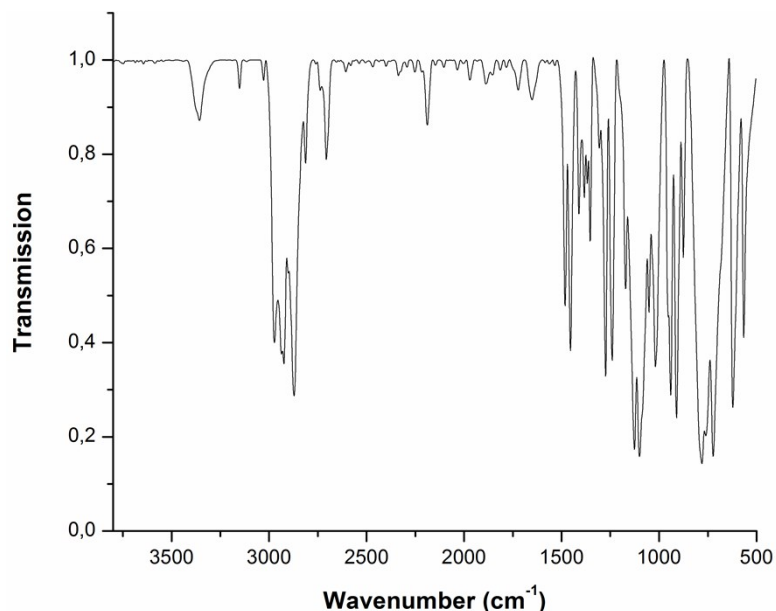


*Figure S13. FT-IR spectra of 1-(3-bromopropyl)silatrane.*

### 1.3.2. Synthesis of 1-(3-azidopropyl)silatrane

The preparation of 1-(3-azidopropyl)silatrane was achieved by dissolving 1-(3-bromopropyl)silatrane (4.5 g, 15 mmol) and sodium azide (3.0 g, 46 mmol) in anhydrous DMSO (30 mL) (Figure S14). The reaction mixture was then subjected to stirring at 70 °C for 48 h. In the next step, the reaction mixture was cooled to room temperature, dissolved in deionized water (250 mL) and extracted three times in chloroform (50 mL). The organic phases were joined, dried over anhydrous magnesium sulphate, filtered and vacuum distilled, yielding 3.44 g of white crystals (88% yield).

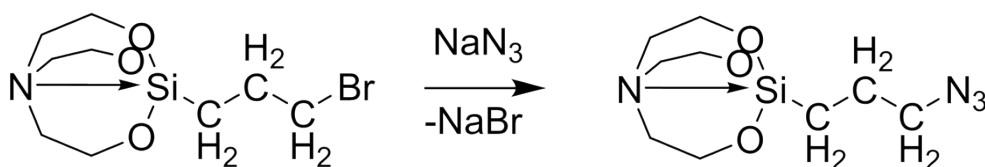


*Figure S14. Schematic representation of 1-(3-azidopropyl)silatrane synthesis.*

$^1\text{H}$  NMR (DMSO- $d_6$ , 400.13 MHz,  $\delta$  (ppm)): 0.17-0.22 (2H, m,  $\text{CH}_2\text{-Si}$ ), 1.53-1.60 (2H, m,  $\text{CH}_2\text{-CH}_2\text{-Si}$ ), 2.80 (6H, t, 5.9 Hz,  $\text{CH}_2\text{-N}$ ), 3.15 (2H, t, 7.2 Hz,  $\text{CH}_2\text{-N}_3$ ), 3.62 (6H, t, 5.9 Hz,  $\text{CH}_2\text{-O}$ ).

$^{13}\text{C}$  NMR (DMSO- $d_6$ , 100.61 MHz,  $\delta$  (ppm)): 14.2 ( $\text{CH}_2\text{-Si}$ ), 24.9 ( $\text{CH}_2\text{-CH}_2\text{-Si}$ ), 49.9 ( $\text{CH}_2\text{-N}$ ), 53.9 ( $\text{CH}_2\text{-N}_3$ ), 56.6 ( $\text{CH}_2\text{-O}$ ).

Both  $^1\text{H}$  and  $^{13}\text{C}$ -NMR spectra of azidopropyl derivative (see Figures S15 and S16) are very similar with those of bromopropyl derivative. The presence of  $\text{N}_3$  moiety is indirectly proven by its influence upon the chemical shift value of the  $^{13}\text{C}$  signal, corresponding to the  $\text{CH}_2$  group directly linked to it. Thus, a 15 ppm downfield shift was observed for this  $\text{CH}_2$  signal of azido derivative, as compared to the brominated derivative.

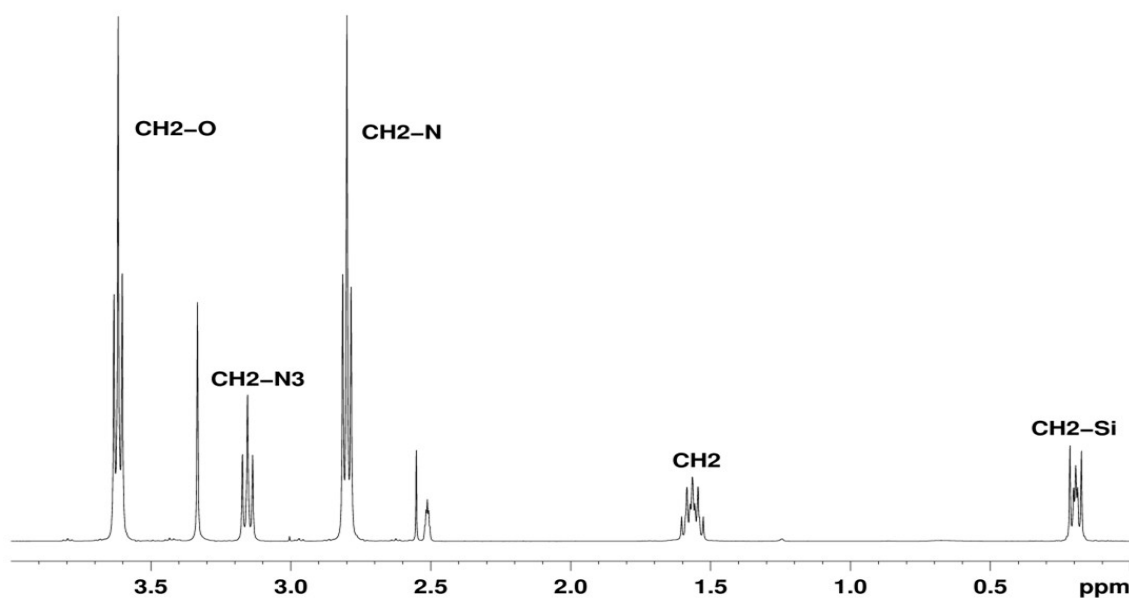


**Figure S15.**  $^1\text{H}$ -NMR spectrum of 1-(3-azidopropyl)silatrane recorded in DMSO- $d_6$ .

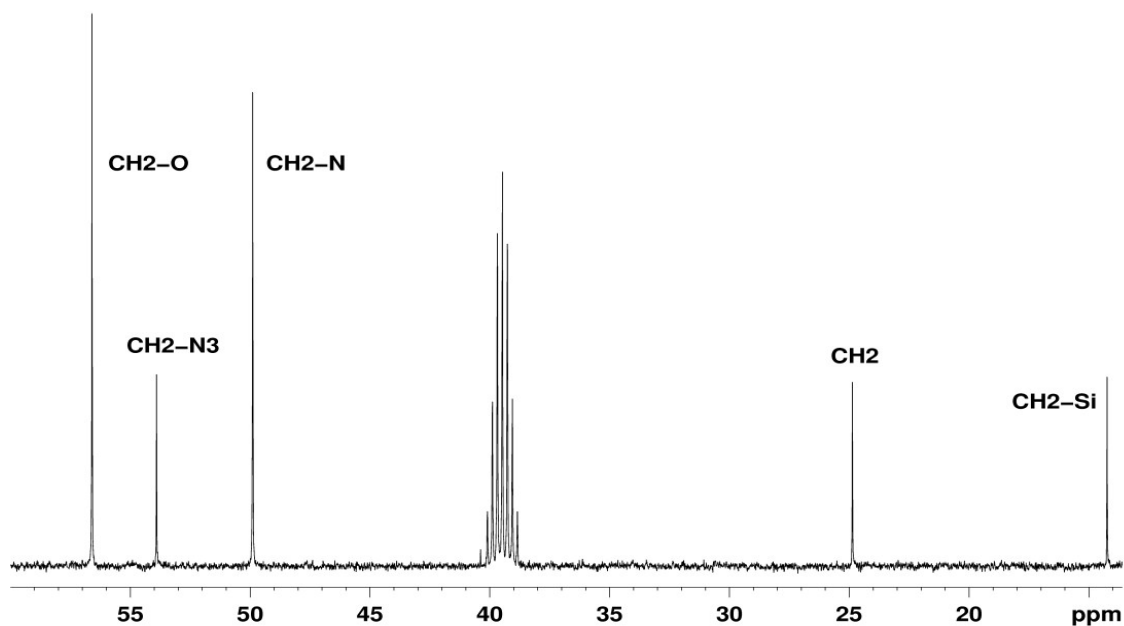


**Figure S16.**  $^{13}\text{C}$ -NMR spectrum of 1-(3-azidopropyl)silatrane recorded in DMSO- $d_6$ .

The strong band at  $2092\text{ cm}^{-1}$  in the FT-IR spectra of the 1-(3-azidopropyl)silatrane (Figure S17) is attributed to the asymmetric vibration of the azide group  $\text{N}_3$ .

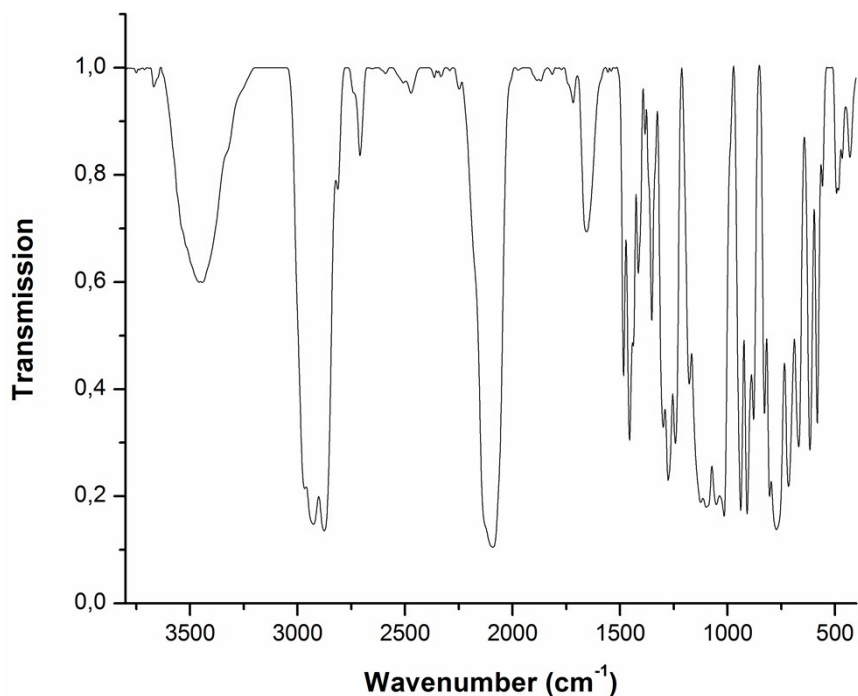


**Figure S17.** FT-IR spectra of 1-(3-azidopropyl)silatrane.

#### 1.4. Synthesis of $\alpha,\omega$ -bis(propargyloxy)poly(ethylene glycol)/acrylated $\beta$ -CD poly(pseudorotaxane)

The preparation of  $\alpha,\omega$ -bis-(propargyloxy)-PEG<sub>1000</sub>/acrylated  $\beta$ -CD poly(pseudorotaxane) was achieved by dissolving  $\alpha,\omega$ -bis-(propargyloxy)-PEG<sub>1000</sub> (0.68 g, 0.67 mmol) and acrylated  $\beta$ -CD (7.0 g, 4.7 mmol) in an acetone/deionized water 1:1 mixture (30 mL) at room temperature under continuous stirring for 72 h (Figure S18).<sup>3</sup> The resulting precipitate was filtered, washed with deionized water (3x7 mL) and acetone (7x7 mL) and dried under vacuum at 50 °C for 24 h, yielding 6.7 g of white powder (87.23% yield).

<sup>1</sup>H NMR (DMSO-d<sub>6</sub>, 400.13 MHz,  $\delta$  (ppm)): 3.43 (2H, t, 2.4 Hz, CH-propargyl), 3.46-3.73 (all -CH<sub>2</sub>-CH<sub>2</sub>-O- from PEO overlapped with H-4 from cyclodextrin), 3.74-4.12 (H-3 and H-2 from cyclodextrin), 4.15 (4H, d, 2.4 Hz, CH<sub>2</sub>-propargyl), 4.12-4.64 (H-5, H-6 and unreacted OH-6 from cyclodextrin), 4.80-5.32 (H-1 from cyclodextrin), 5.80-6.50 (OH-2, OH-3 from cyclodextrin and acrylic protons).

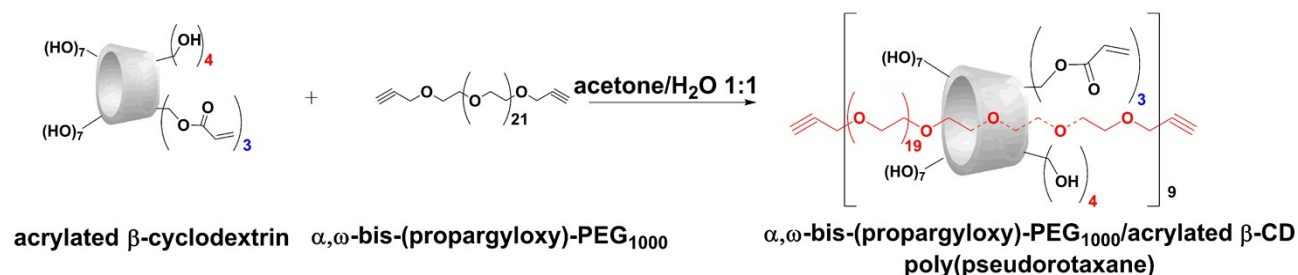


**Figure S18.** Schematic representation of  $\alpha,\omega$ -bis-(propargyloxy)-PEG<sub>1000</sub>/acrylated  $\beta$ -CD poly(pseudorotaxane) preparation.

The <sup>1</sup>H-NMR spectrum of the obtained pseudorotaxane is complex (Figure S19), with very broad signals characteristic to the acrylated  $\beta$ -cyclodextrin, and resolved signals characteristic to PEG-propargyl moiety. The PEG-propargyl moiety has 3 distinctive signals: a triplet centred at 3.43 ppm assigned to the two CH from propargyl, a broad singlet at 3.52 ppm assigned to all CH<sub>2</sub> from PEO and a doublet at 4.15 ppm assigned to the two CH<sub>2</sub> from propargyl. In the <sup>1</sup>H NMR spectrum, the integral ratio between the **H-1** protons from cyclodextrin and CH<sub>2</sub> protons from propargyl is 64.3 : 4, indicating 9 acrylated  $\beta$ -cyclodextrins units on the PEG axle (the  $\beta$ -cyclodextrin molecule has 7 protons in **1** position, 64.3 divided to 7 results in 9.1 cyclodextrin molecules).

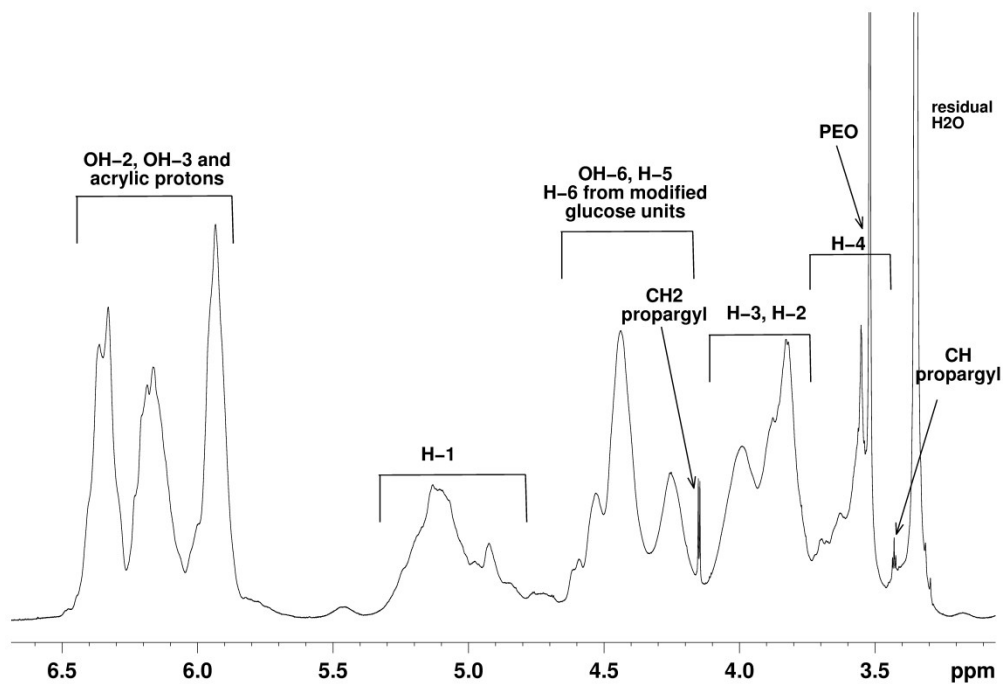


**Figure S19.**  $^1\text{H-NMR}$  spectrum of the prepared  $\alpha,\omega$ -bis-(propargyloxy)-PEG<sub>1000</sub>/acrylated  $\beta$ -CD poly(pseudorotaxane), recorded in DMSO-*d*<sub>6</sub>.

The FT-IR spectra of the poly(pseudorotaxane) comprised of  $\alpha,\omega$ -bis-(propargyloxy)-PEG<sub>1000</sub> as “guest” and partially acrylated  $\beta$ -CD as “host” revealed the characteristic bands corresponding to the components (Figure S20). One can observe the absorption band of the remaining hydroxyl groups centred at  $3477\text{ cm}^{-1}$ , alongside the methylene groups at  $2927\text{ cm}^{-1}$ . The strong absorption band at  $1728\text{ cm}^{-1}$  is due to the presence of the C=O carbonyl groups inserted during the esterification of the primary hydroxyl groups with acryloyl chloride.

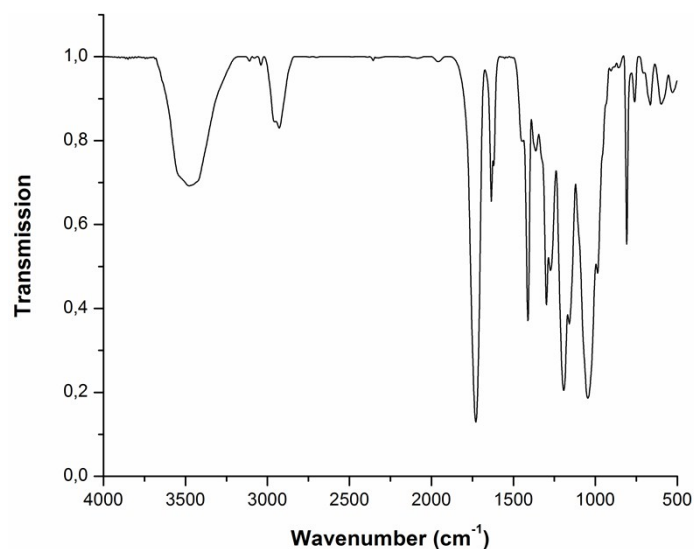


**Figure S20.** FT-IR spectra of  $\alpha,\omega$ -bis-(propargyloxy)-PEG<sub>1000</sub>/acrylated  $\beta$ -CD poly(pseudorotaxane).

### 1.5. Preparation of $\alpha,\omega$ -bis-{1-[3-(silatranyl)prop-1-yl]-1H-1,2,3-triazol-5-yl]-PEG<sub>1000</sub>/acrylated $\beta$ -CD polyrotaxane (ROT)

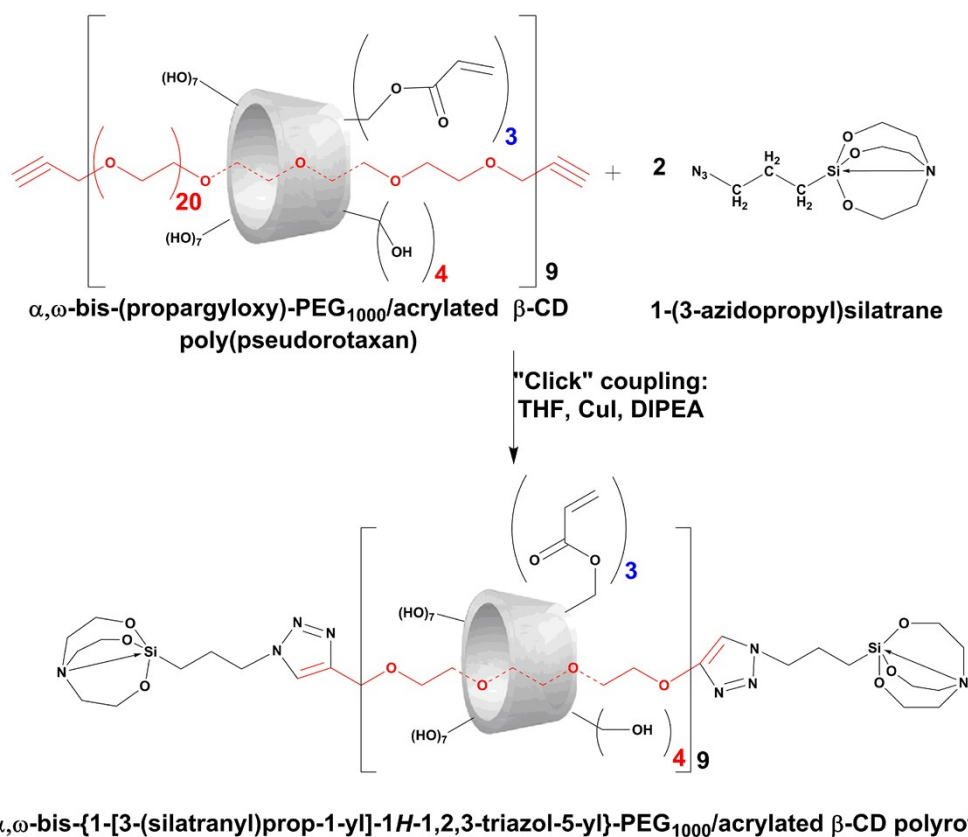


**Figure S21.** Schematic representation of  $\alpha,\omega$ -bis-{1-[3-(silatranyl)prop-1-yl]-1H-1,2,3-triazol-5-yl}-PEG<sub>1000</sub>/acrylated  $\beta$ -CD polyrotaxane synthesis procedure.

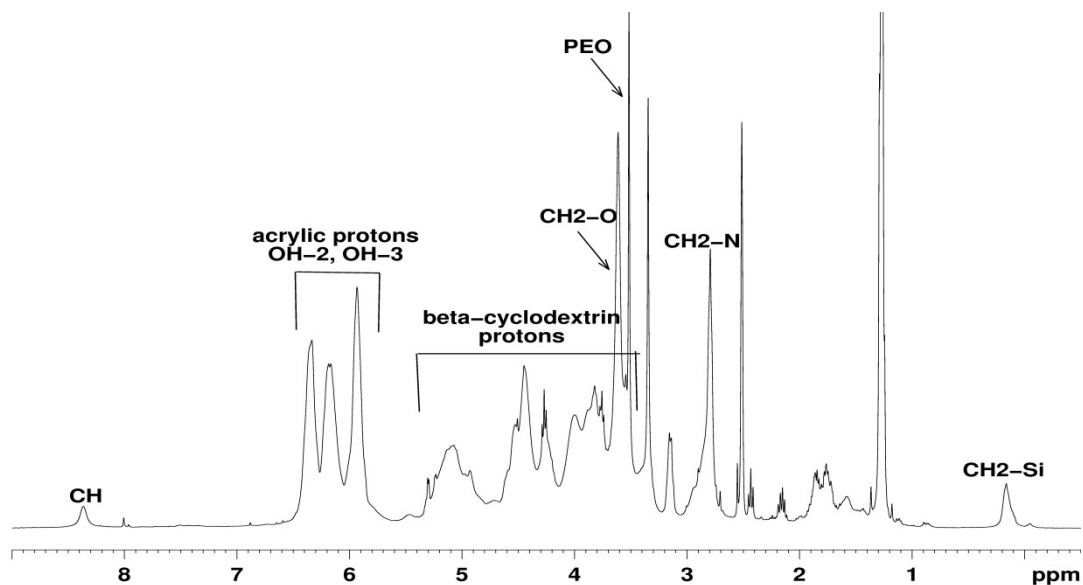


**Figure S22.**  $^1\text{H-NMR}$  spectrum of the capped ROT, recorded in  $\text{DMSO-d}_6$ .

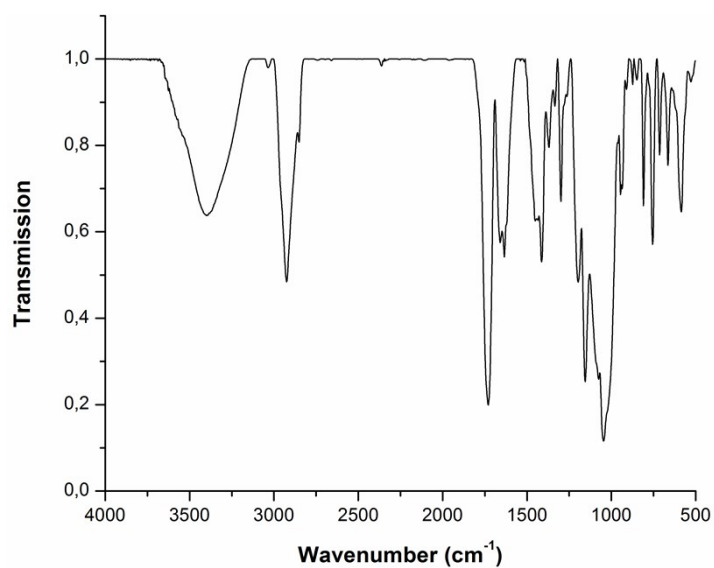


**Figure S23.** FT-IR spectra of  $\alpha,\omega$ -bis- $\{1-[3-(\text{silatranyl})\text{prop-1-yl}]-1\text{H-1,2,3-triazol-5-yl}\}$ - $\text{PEG}_{1000}/\text{acrylated } \beta\text{-CD polyrotaxane}$ .

## 1.6. Preparation of PEI decorated polyrotaxane (ROT-PEI)

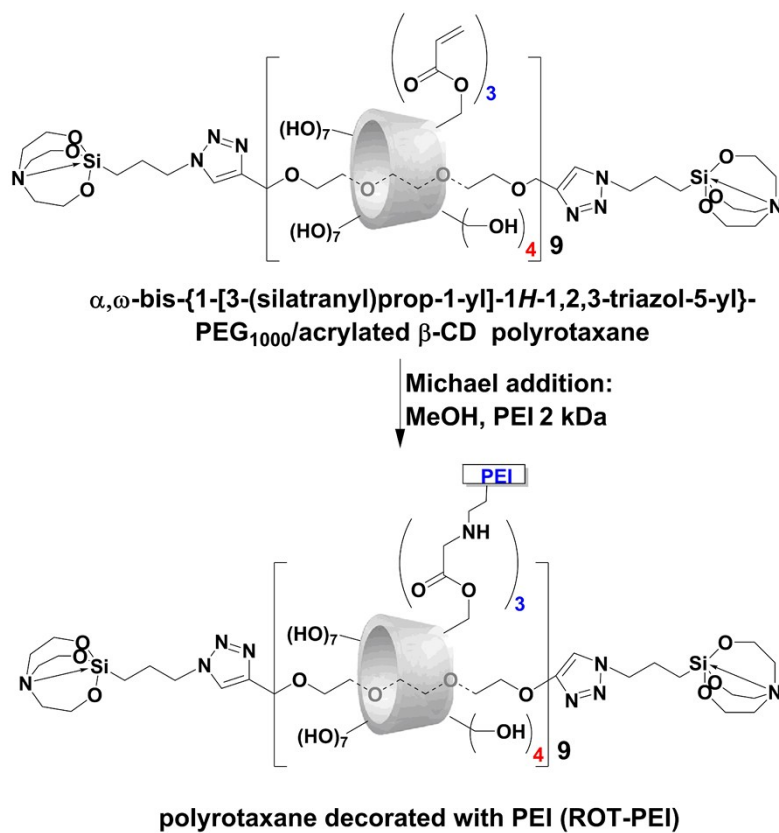
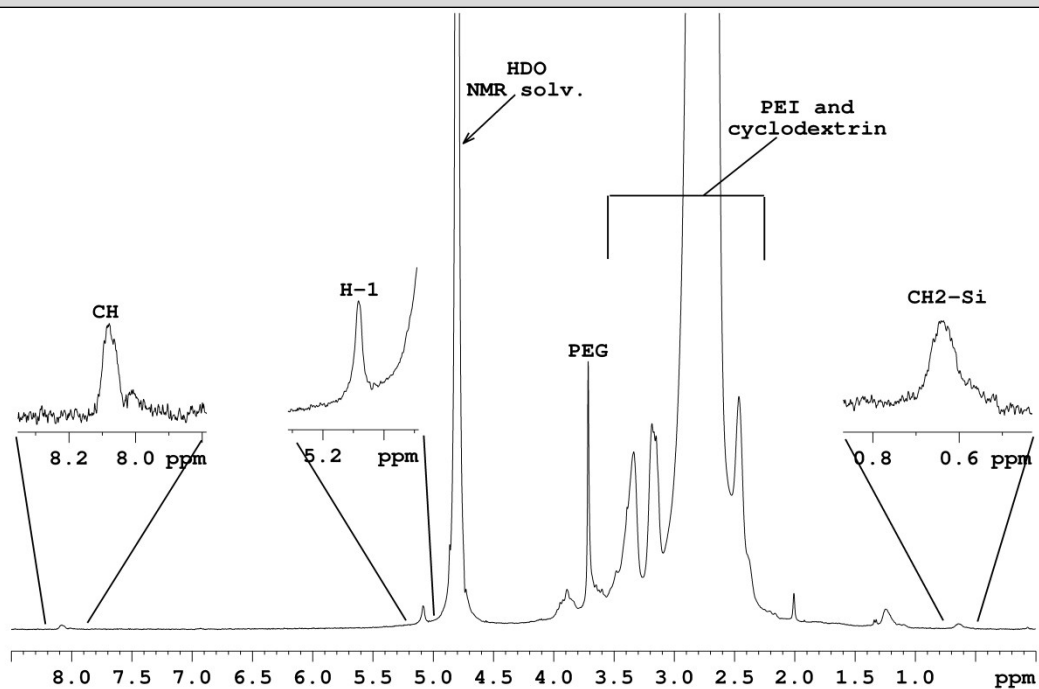
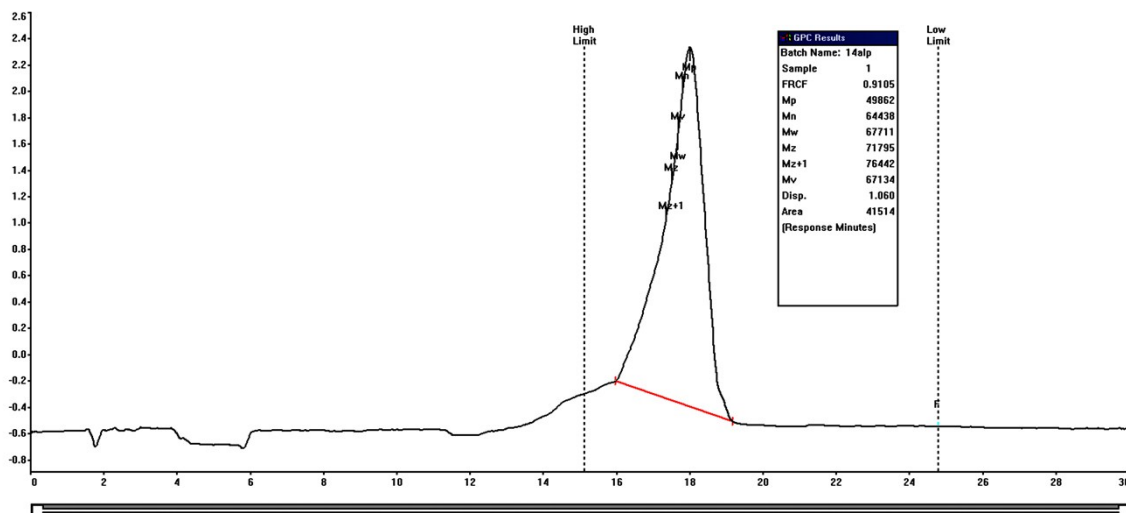


Figure S24. Schematic representation of ROT-PEI preparation.



**Figure S25.**  $^1\text{H-NMR}$  spectrum of ROT-PEI, recorded in  $\text{D}_2\text{O}$ .



**Figure S26.** The GPC curve of ROT-PEI product in water. Calibration was performed by using the Agilent PEO calibration kit (polyethylene oxide).

### 1.7. Preparation of PEI and PEG<sub>750</sub> decorated polyrotaxane (ROT-PEI-PEG<sub>750</sub>)

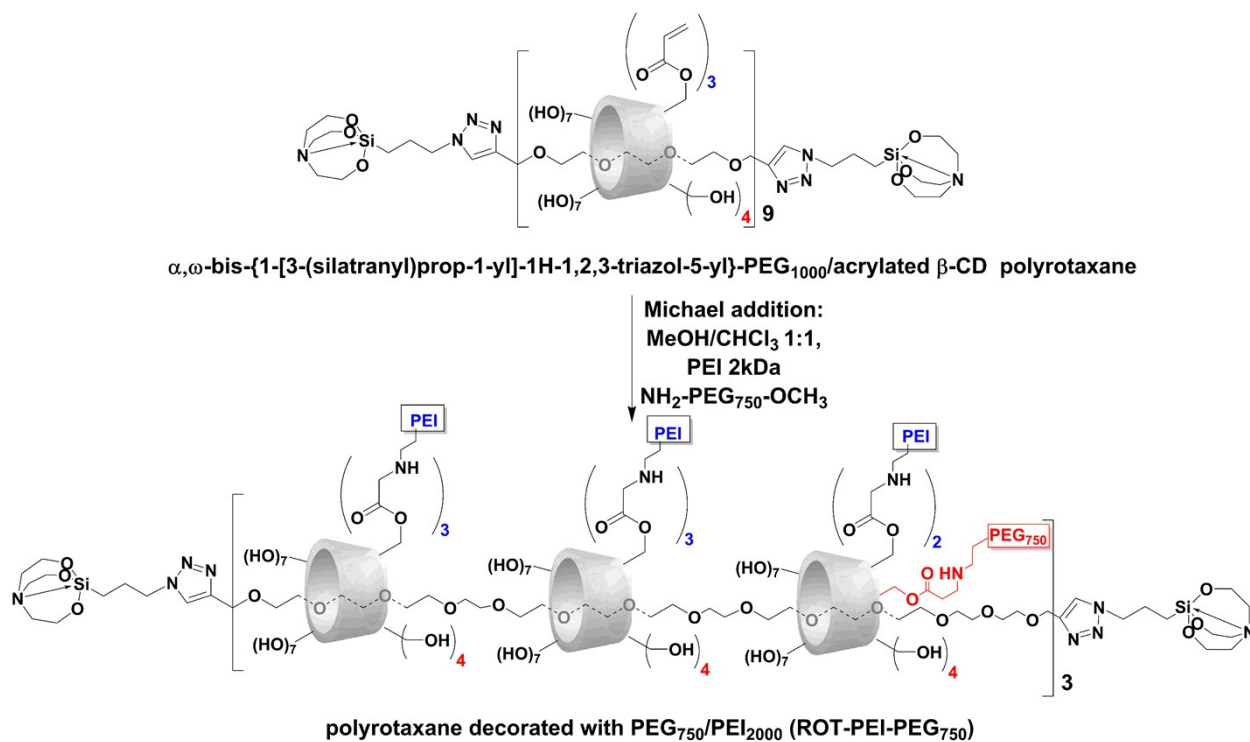


**Figure S27.** Schematic representation of ROT-PEI-PEG<sub>750</sub> preparation.

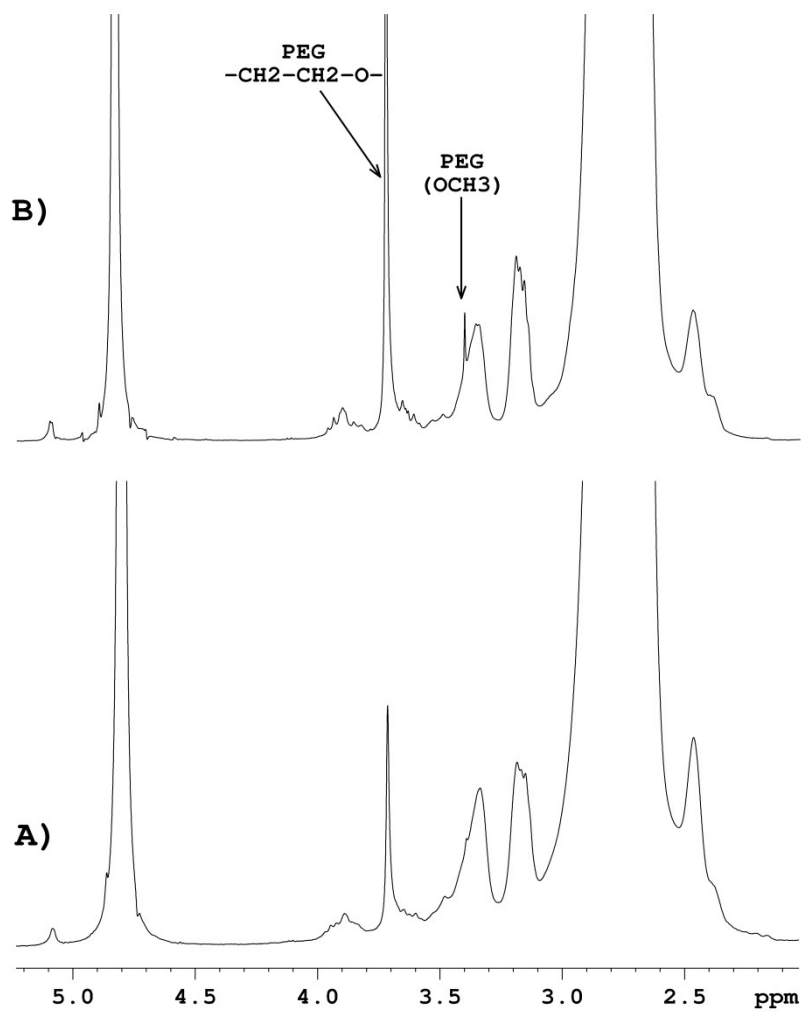


**Figure S28.** <sup>1</sup>H-NMR spectra of **A)** ROT-PEI and **B)** ROT-PEI-PEG<sub>750</sub>, both recorded in D<sub>2</sub>O. Only the region characteristic to PEI and PEG is displayed.

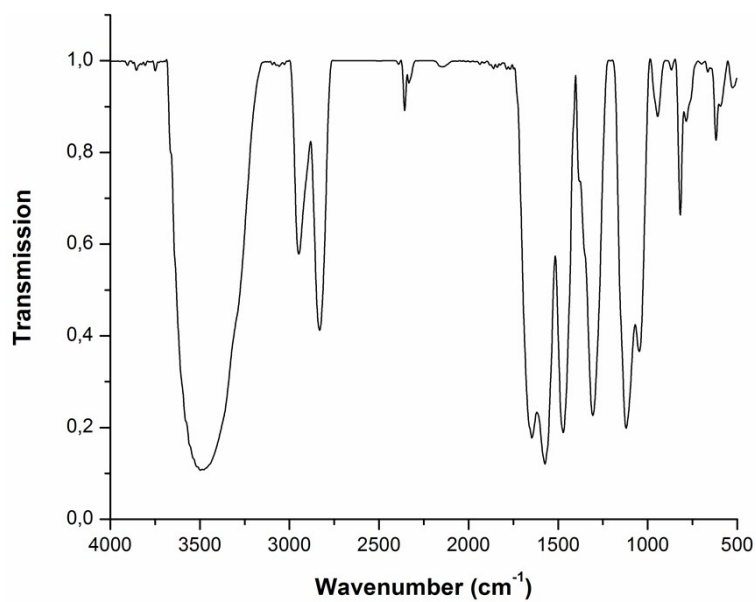


**Figure S29.** FT-IR spectrum of ROT-PEI-PEG<sub>750</sub>.

### 1.8. Preparation of arginine decorated ROT-PEI (ROT-PEI-Arg)

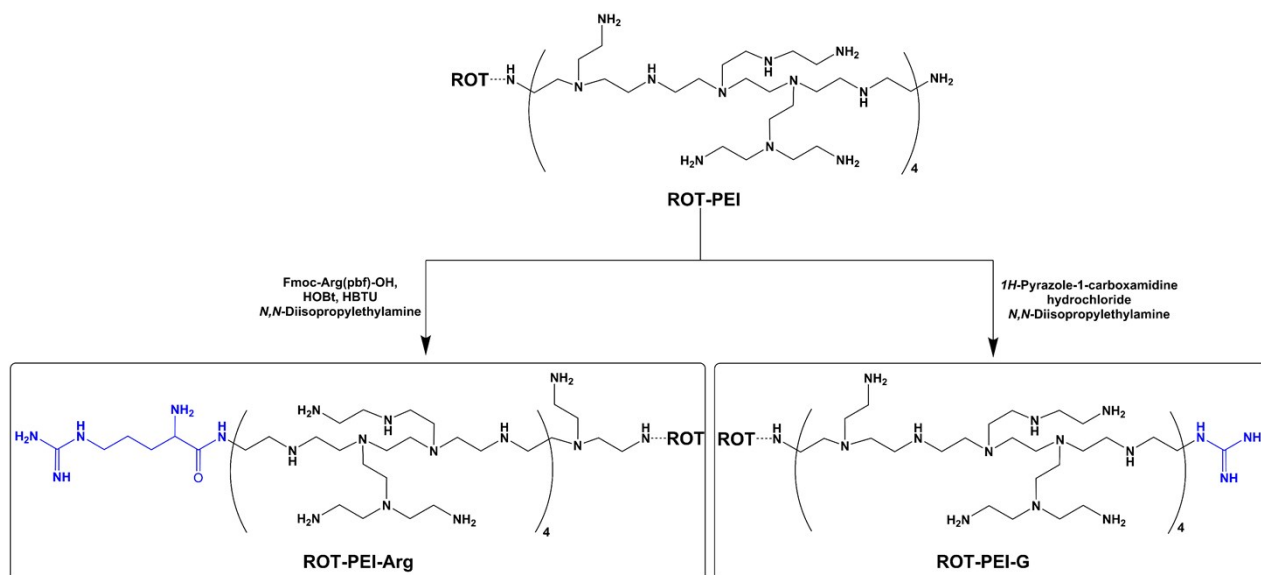


**Figure S30.** General reaction pathway of ROT-PEI-Arg and ROT-PEI-G preparation.

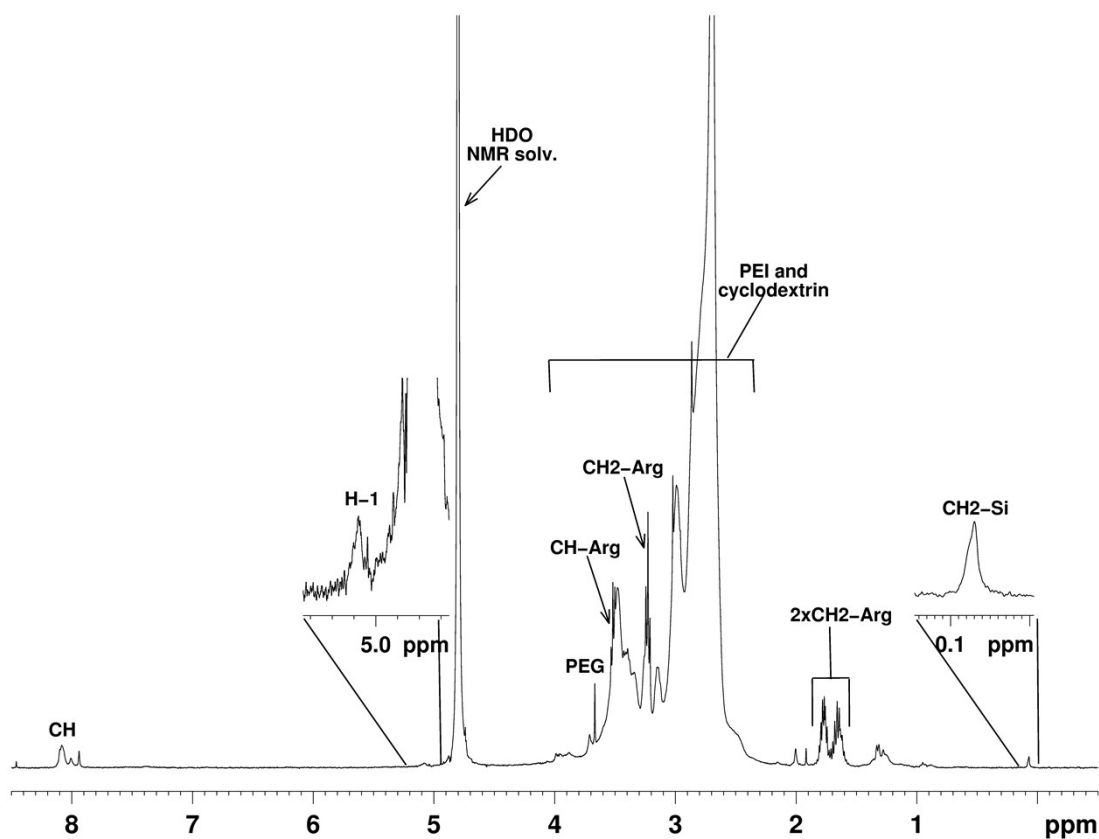


**Figure S31.**  $^1\text{H}$ -NMR spectrum of ROT-PEI-Arg, recorded in  $\text{D}_2\text{O}$ .

### 1.9. Preparation of guanidine decorated ROT-PEI (ROT-PEI-G)

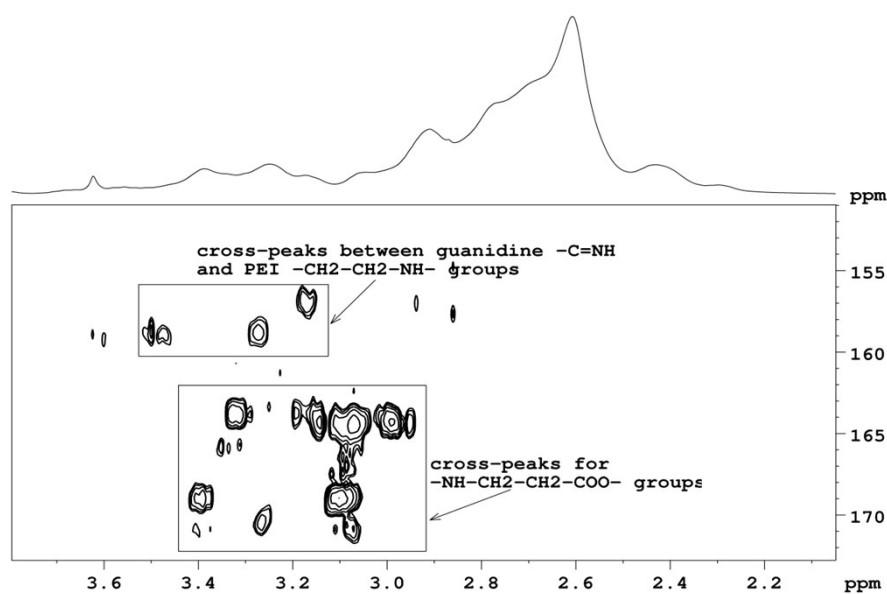


**Figure S32.**  $^1\text{H}$ ,  $^{13}\text{C}$ -HMBC spectrum of ROT-PEI-G, recorded in  $\text{D}_2\text{O}$ . Only the regions of interest are displayed  $^1\text{H}$ : 2.0-3.8 ppm and  $^{13}\text{C}$ : 150-173 ppm.

## 2. Elemental analysis of the investigated carriers

*Table S1. Elemental composition of the investigated carriers [mass %].*

Investigated carrier	Chemical element [mass %]			
	C	N	O	Si
<b>ROT-PEI</b>	52.05	28.35	9.19	0.087
<b>ROT-PEI-PEG<sub>750</sub></b>	52.03	26.71	10.97	0.092
<b>ROT-PEI-G</b>	51.69	28.81	9.26	0.082
<b>ROT-PEI-Arg</b>	51.64	29.01	9.03	0.085

### 3. *In silico* chemical modeling

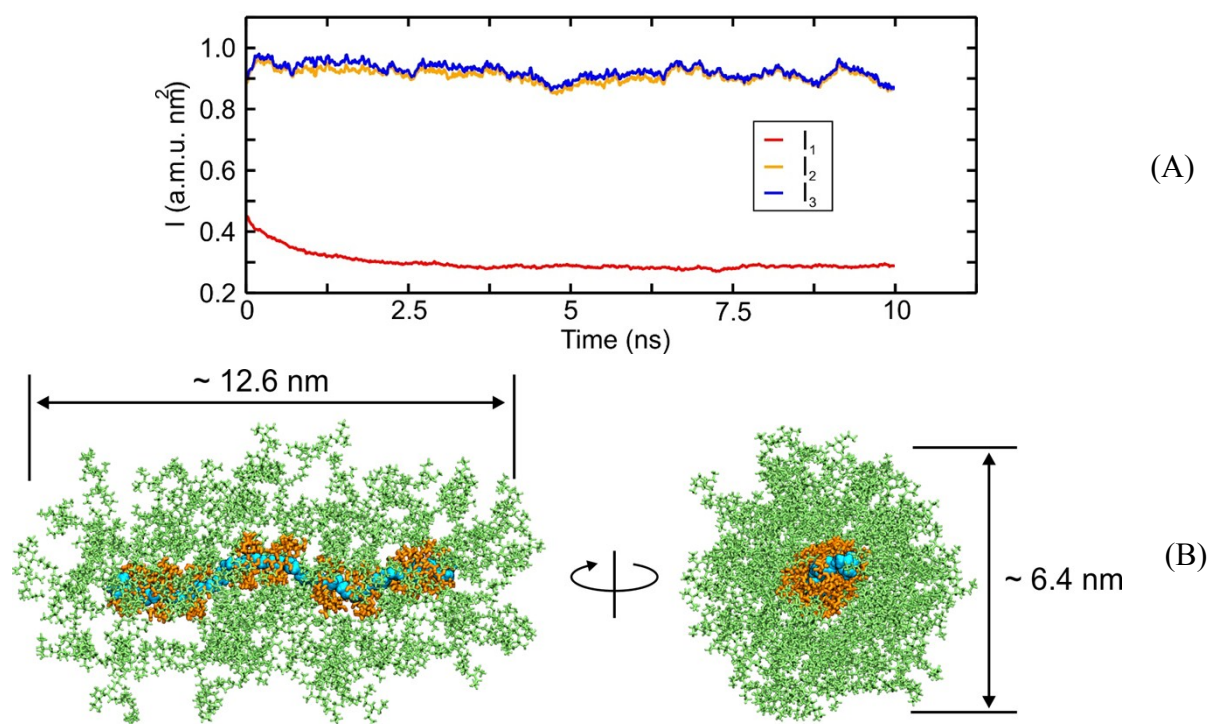


**Figure S33.** (A) Moment of inertia (MOI) variation during the production molecular dynamics simulation, as a measure of system equilibration.  $I_x$ ,  $I_y$ ,  $I_z$  – MOI around the principal axes of the polyrotaxane aggregate. ‘Z’ axis is oriented along the longitudinal PEG/stopper direction. (B) Snapshot of the structure of the polyrotaxane aggregate at the end of the 10 ns MD simulation.

PEI (green),  $\beta$ -CD (orange), and PEG/stopper (cyan).

#### 4. The efficacy of carriers – dsDNA electrostatic complexation (Gel retardation assay)

Cargocomplexes prepared at precise N/P ratios, were mixed with loading buffer (1X TAE buffer, pH 7.4) and then loaded in a 1% agarose gel. Electrophoresis was carried out at 90 V, for 120 minutes, in TAE running buffer solution (40 mM Tris-HCl, 1% glacial acetic acid, 1 mM EDTA). The migration of partially complexed plasmid towards anode was visualized under UV light, by staining with ethidium bromide. Figure S34 depicts the results of gel retardation assay.

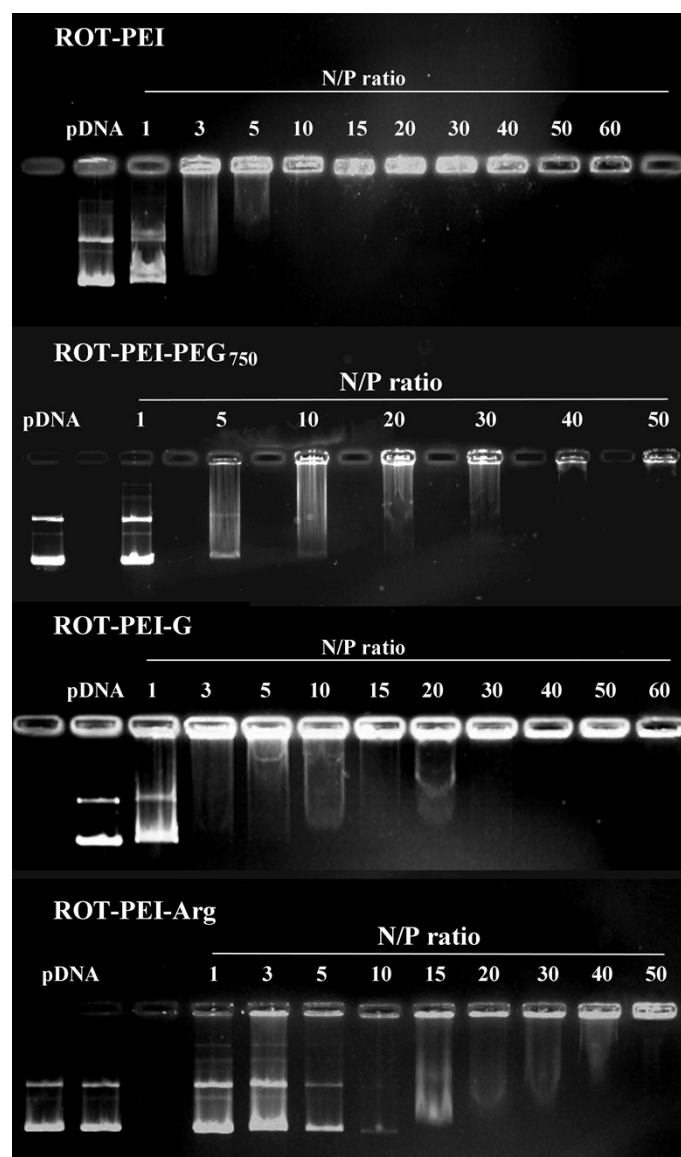
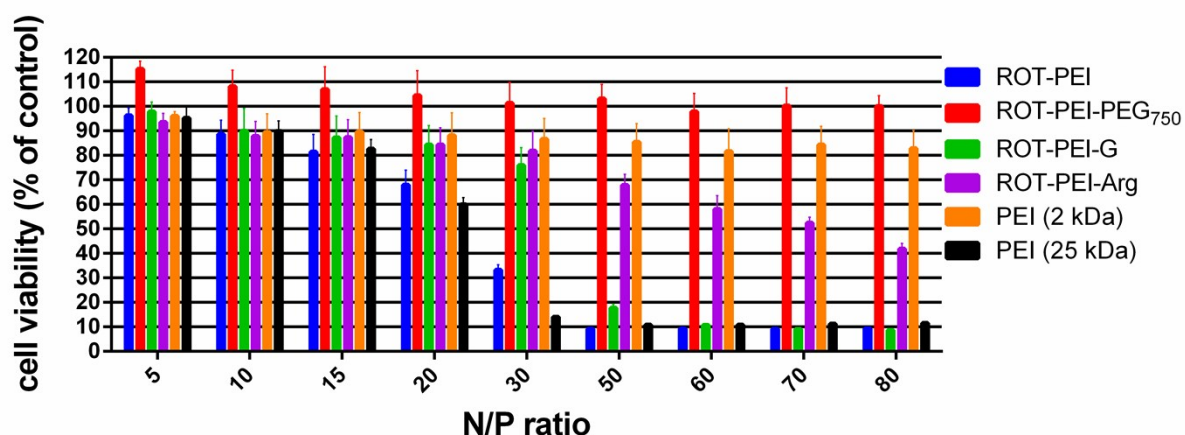


**Figure S34.** Gel retardation assay of ROT-PEI/pDNA, ROT-PEI-PEG<sub>750</sub>/pDNA, ROT-PEI-G/pDNA, ROT-PEI-Arg/pDNA polyplexes at various N/P ratios from 1 to 60.

## 5. Cytotoxicity assay

Cytotoxicity was measured using MTS technique (CellTiter 96® Aqueous One Solution Cell Proliferation Assay, Promega) which measures the mitochondrial reductase activity.<sup>4</sup> HeLa cells were seeded at a density of 104 cells per well in 96 well plates, in 100  $\mu$ L complete medium. The next day, cells were transfected with polyplexes as described above, after which the cells were grown for another 44 hours. At least 8 biological replicates were performed for each polyplex type and N/P ratio, and each experiment was repeated 3 times. After 44 hours, 20  $\mu$ L of CellTiter 96® Aqueous One Solution reagent were added to each well, and the plates were incubated for another 4 hours before reading the result. Absorbance at 490 nm was recorded with a plate reader (EnSight, PerkinElmer).

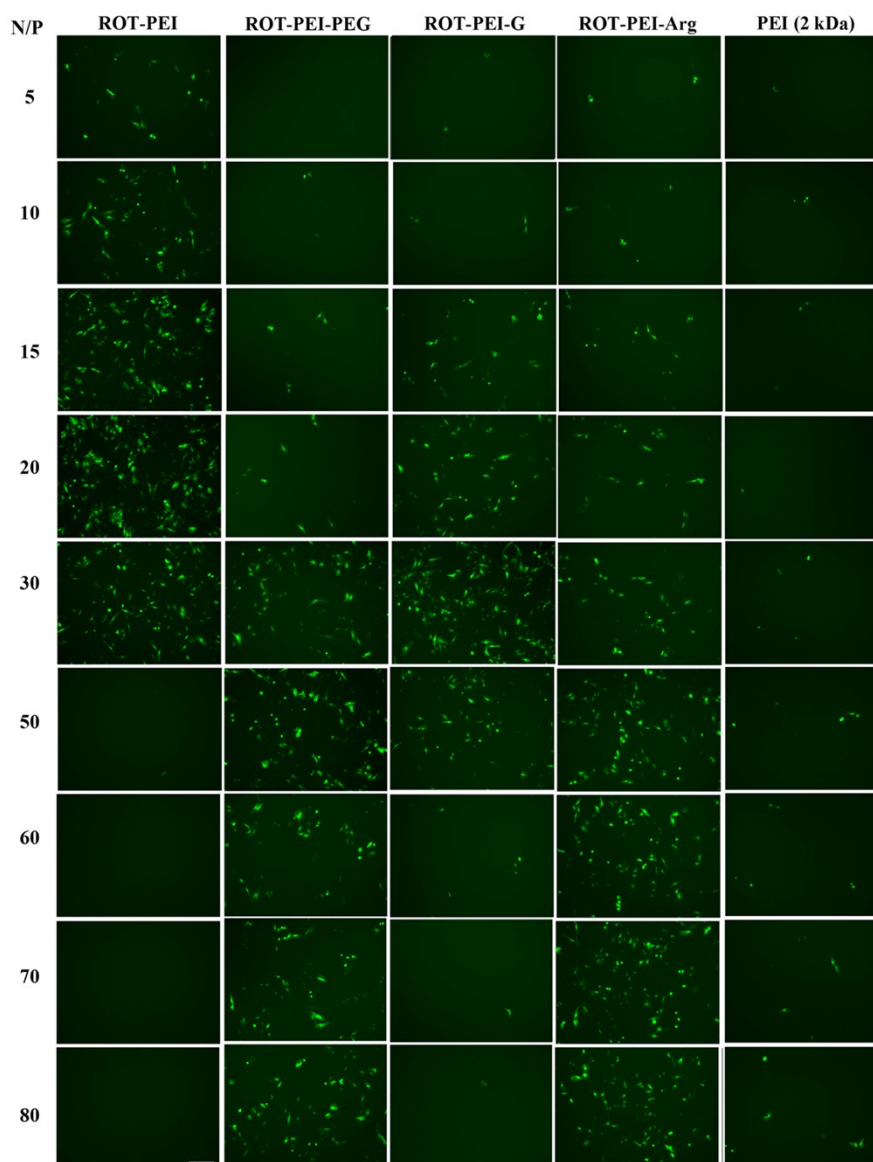
According to MTS assay results (Figure S35), the PEG-ylated compound, ROT-PEI-PEG<sub>750</sub> displays the highest cell viability of approximately 100%, inducing cell proliferation at small N/P ratios. The other tested vehicles show a cellular viability higher than 70% at the N/P of maximum transfection yield.



**Figure S35.** The results of cytotoxicity tests in the series of investigated transfection agents.

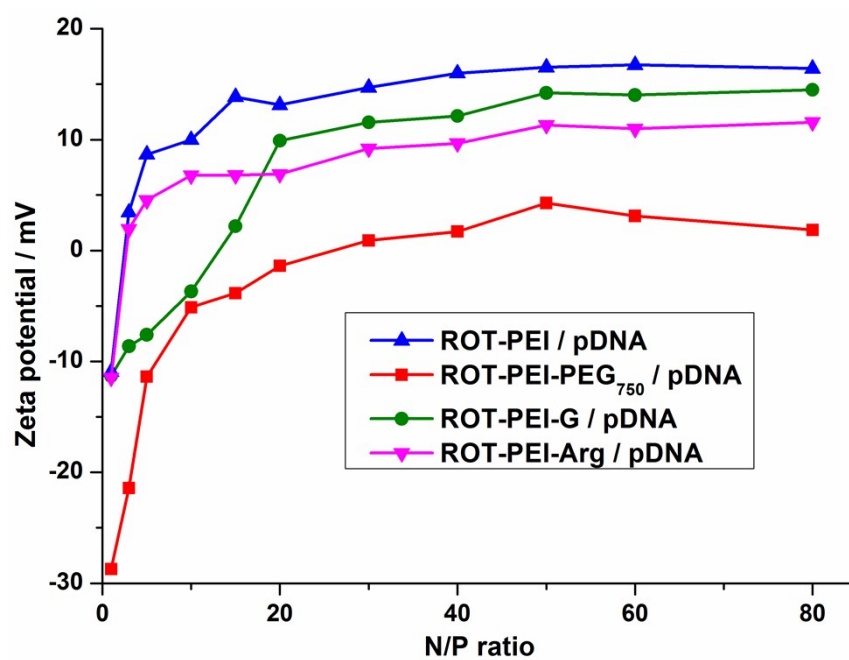
## 6. Transfection efficacy tests

Figure S36 depicts the transfection capacity and abundance of the transfected cells using different carriers, at various N/P ratios.



**Figure S36.** Fluorescence microscopy images of GFP-transfected cells, using ROT-PEI/pGFP, ROT-PEI-PEG<sub>750</sub>/pGFP, ROT-PEI-G/pGFP, ROT-PEI-Arg/pGFP and PEI (2 kDa)/pGFP as transfection agents, at all tested N/P ratios (from 5 to 80).

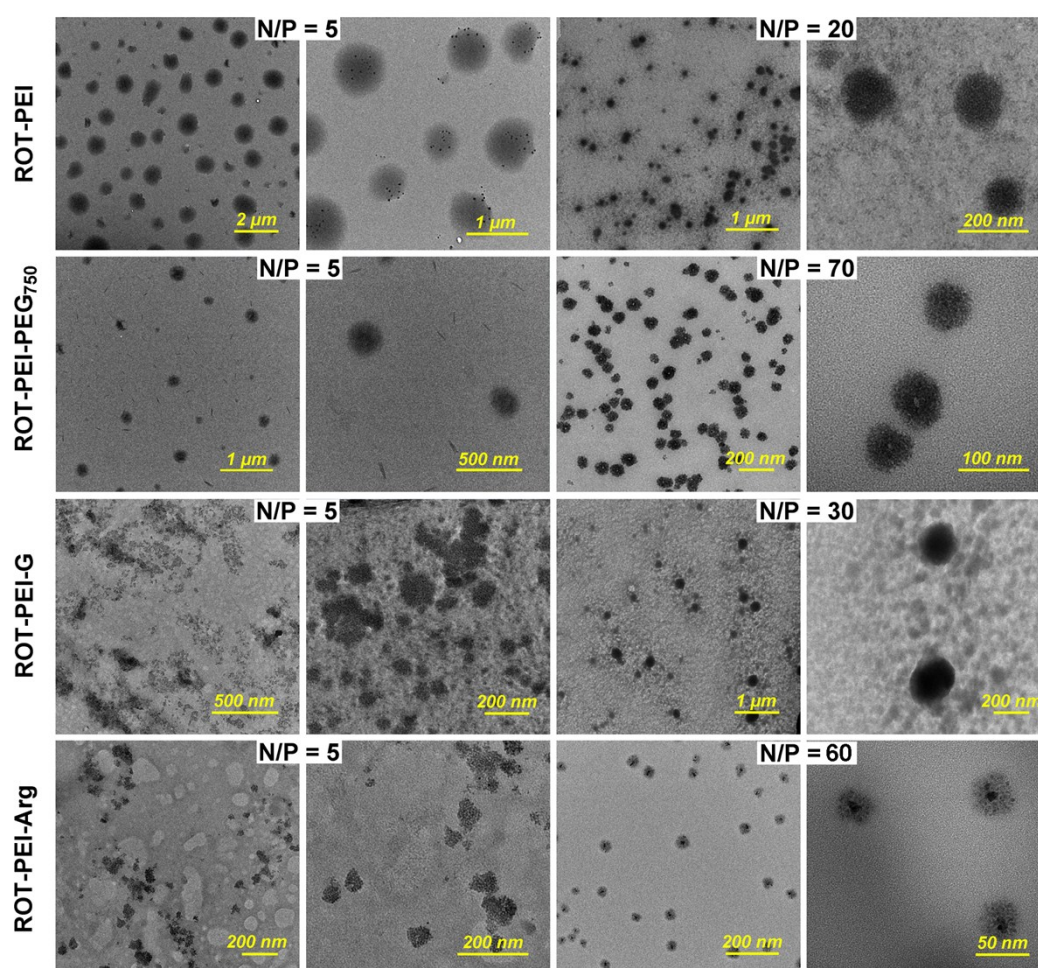
## 7. Zeta potential measurements of polyplexes



**Figure S37.** The zeta potential variation of ROT-PEI/pDNA, ROT-PEI-PEG<sub>750</sub>/pDNA, ROT-PEI-G/pDNA and ROT-PEI-Arg/pDNA polyplexes prepared at N/P ratios ranging from 1 to 80, buffered at pH 7.4, in aqueous media.

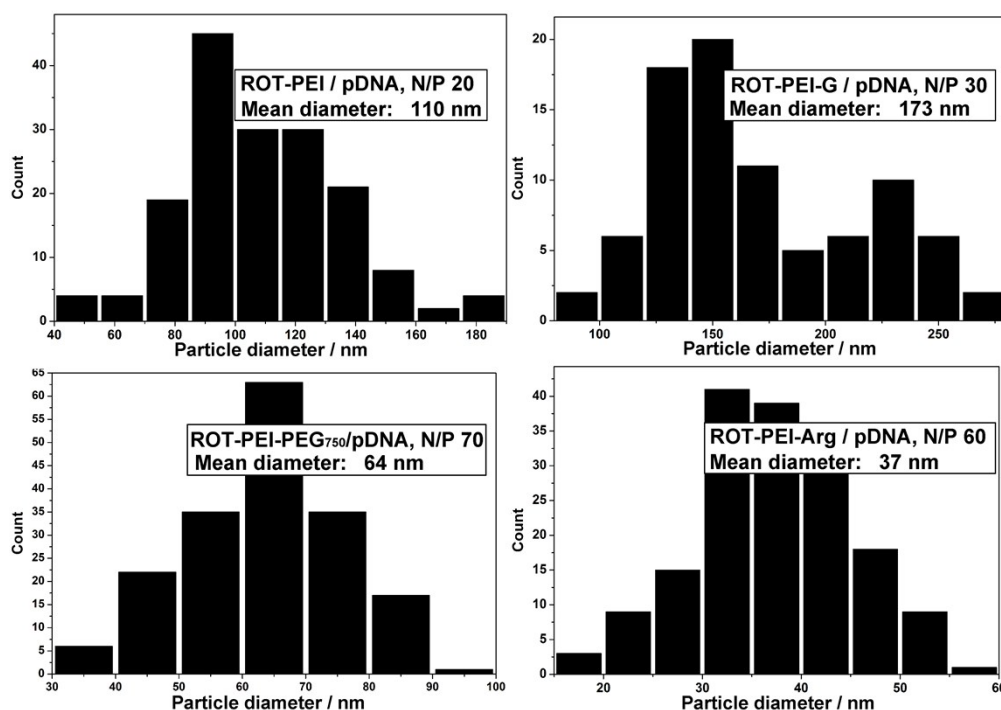
## 8. Transmission electron microscopy (TEM)

Figure S38 shows TEM images of rotaxane based polyplexes at two N/P ratios for each system: one for which transfection begins to be noticed in almost all vectors (N/P 5) and another N/P when the maximum transfection efficiency was observed: 20, 70, 30 and 60 for ROT-PEI, ROT-PEI-PEG<sub>750</sub>, ROT-PEI-G, ROT-PEI-Arg, respectively. One can see that at N/P 5 ROT-PEI/pDNA and ROT-PEI-PEG<sub>750</sub>/pDNA polyplexes begin to organize in spherical entities, unlike ROT-PEI-G/pDNA and ROT-PEI-Arg/pDNA polyplexes that present the formation of irregularly shaped entities. Well defined particles of spherical morphology have been obtained at N/P ratios of higher transfection yields.



**Figure S38.** TEM images of ROT-PEI/pDNA, ROT-PEI-PEG<sub>750</sub>/pDNA, ROT-PEI-G/pDNA and ROT-PEI-Arg/pDNA polyplexes, at two N/P ratios: one N/P at which the transfection was very low (N/P 5), and another one for the highest transfection yield, which is different for each particular system, 20, 70, 30, and 60 respectively.

Based on TEM images, the mean diameters of polyplexes were determined (Figure S39). The smallest value of average particle diameter was found in ROT-PEI-Arg/pDNA at N/P 60 (37 nm), followed by ROT-PEI-PEG<sub>750</sub>/pDNA at N/P 70 (64 nm). ROT-PEI/pDNA and ROT-PEI-G/pDNA polyplexes, developing larger particles, don't exceed 200 nm in diameter, which is desirable when intended for application in a biological environment.



**Figure S39.** Size distribution of polyplex particles, obtained at N/P ratios of maximum transfection efficiency, according to TEM data. The average diameters of ROT-PEI/pDNA (N/P 20), ROT-PEI-PEG<sub>750</sub>/pDNA (N/P 70), ROT-PEI-G/pDNA (N/P 30) and ROT-PEI-Arg/pDNA (N/P 60) were found of 110, 64, 173 and 37 nm respectively.

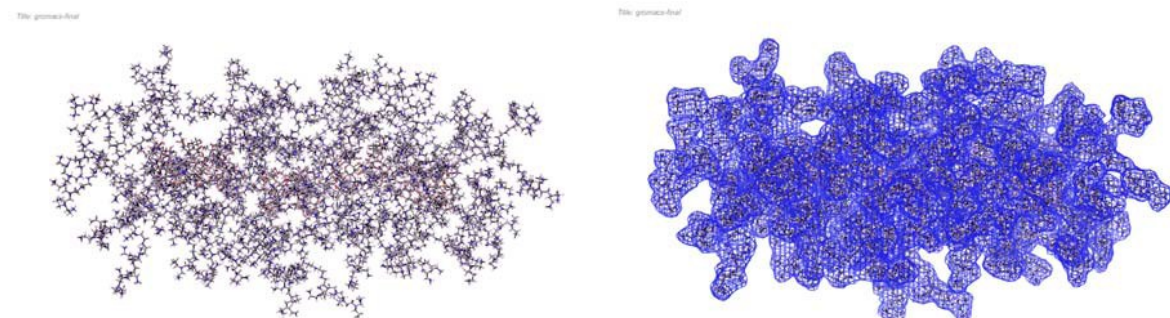
## 9. Size measurements by Dynamic Light Scattering (DLS) analysis

**Table S2.** Size measurements of ROT-PEI/pDNA, ROT-PEI-PEG<sub>750</sub>/pDNA, ROT-PEI-G/pDNA and ROT-PEI-Arg/pDNA polyplexes at maximum transfection efficiency, obtained by DLS.

<b>Investigated polyplex (N/P ratio)</b>	<b>Particle size (nm)</b>	<b>Polydispersity index</b>
<b>ROT-PEI/pDNA (N/P: 20)</b>	<b>131.5 ± 34.9</b>	<b>0.229</b>
<b><i>ROT-PEI-PEG<sub>750</sub>/pDNA</i> (N/P: 70)</b>	<b>232.7 ± 61.9</b>	<b>0.422</b>
<b>ROT-PEI-G/pDNA (N/P: 30)</b>	<b>219.2 ± 33.7</b>	<b>0.169</b>
<b>ROT-PEI-Arg/pDNA (N/P: 60)</b>	<b>93.9 ± 10.6</b>	<b>0.437</b>

## 10. The *in silico* estimation of the volume of cargocomplexes

A



B

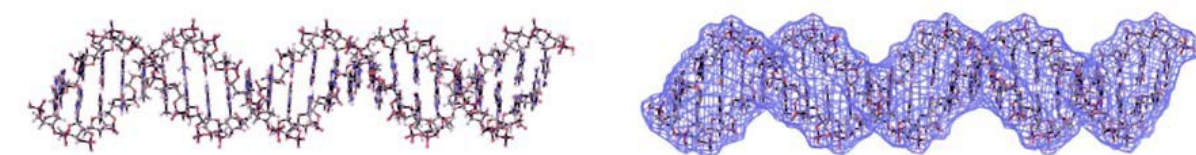


**Figure S40.** The results of the calculation Van der Waals lateral surfaces enclosing the ROT-PEI polyrotaxane carrier, and the Dickerson-Drew DNA dodecamer.

## References

1. P. Rolling, M. Lamers, C. Staudt, *J. Membr. Sci.* **2010**, 362, 154.
2. a) M. G. Voronkov and V. M. Dyakov, *United States Patent 4048206*, Sept. 13, **1977**; b) R. Singh, J. Kishore Puri, R. P. Sharma, A. K. Malik, V. Ferretti, *J. Mol. Struct.* **2010**, 982, 107.
3. Q. Fu, J. M. Ren, S. Tan, J. Xu, G. G. Qiao, *Macromol. Rapid Commun.* **2012**, 33(24), 2109.
4. a) J. A. Barltrop, T. C. Owen, A. H. Cory, J. G. Cory, *Bioorg. Med. Chem. Lett.* **1991**, 1, 611; b) I. A. Turin-Moleavin, F. Doroftei, A. Coroaba, D. Peptanariu, M. Pinteala, A. Salic, M. Barboiu, *Org. Biomol. Chem.* **2015**, 13(34), 9005.